


RESEARCH ARTICLE | FEBRUARY 11 2022

Thermocapillary droplet migration in a vertical temperature gradient controlled by thermal radiations

Zuo-Bing Wu (武作兵) 



Physics of Fluids 34, 022109 (2022)

<https://doi.org/10.1063/5.0082867>



View
Online



Export
Citation

CrossMark

Articles You May Be Interested In

Thermocapillary migration of a deformed droplet in the combined vertical temperature gradient and thermal radiation

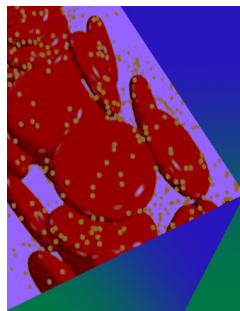
Physics of Fluids (March 2023)

Free convection on heated horizontal circular cylinder in presence of heat generation

AIP Conference Proceedings (June 2014)

Kinematics of Phase Boundary Growth. Directional Solidification

AIP Conference Proceedings (January 2010)



Physics of Fluids

Special Topic: Flow and Forensics

Submit Today!



Thermocapillary droplet migration in a vertical temperature gradient controlled by thermal radiations

Cite as: Phys. Fluids **34**, 022109 (2022); doi: [10.1063/5.0082867](https://doi.org/10.1063/5.0082867)

Submitted: 19 December 2021 · Accepted: 1 February 2022 ·

Published Online: 11 February 2022




View Online



Export Citation



CrossMark

Zuo-Bing Wu (武作兵)^{a)} 

AFFILIATIONS

LNM, Institute of Mechanics, Chinese Academy of Sciences, Beijing 100190, China and School of Engineering Science, University of Chinese Academy of Sciences, Beijing 100049, China

^{a)} Author to whom correspondence should be addressed: wuzb@lnm.imech.ac.cn

ABSTRACT

Thermocapillary migration of a droplet in a vertical temperature gradient controlled by uniform and non-uniform thermal radiations is theoretically analyzed and numerically investigated. A non-dimensionalized thermal radiation number is proposed to quantitatively depict the intensity ratio of the thermal radiation flux to the uniform temperature gradient. From the momentum and energy equations at zero limits of Reynolds and Marangoni numbers, analytical results for the uniform and non-uniform thermal radiations are determined. The steady migration velocity raises with the increasing of the thermal radiation number. By using the front-tracking method, it is observed that thermocapillary droplet migration under the uniform thermal radiation at moderate Marangoni and moderate thermal radiation numbers reaches a steady process. The steady migration velocity decreases with the increasing of Marangoni number and increases with the increasing of thermal radiation number. Moreover, the intensity of thermal energy transferred from the interface to both fluids depends on the volume heat capacity ratio. For the larger/smaller volume heat capacity ratio, more heat is transferred into the continuous phase fluid/the droplet. Furthermore, when the uniform thermal radiation is replaced by the non-uniform ones, the time evolutions, the structures of temperature fields, and parameter dependencies of thermocapillary droplet migration at moderate Marangoni and moderate thermal radiation numbers remain qualitatively unchanged. This study provides a profound understanding of thermocapillary droplet migration in a vertical temperature gradient controlled by thermal radiations, which is of great significance for practical applications in microgravity and microfluidic fields.

Published under an exclusive license by AIP Publishing. <https://doi.org/10.1063/5.0082867>

I. INTRODUCTION

In a microgravity environment, the migration of a droplet in an external fluid caused by the non-uniform surface tension distribution along the interface between two immiscible fluids is termed thermocapillary droplet migration. With the fast development of space exploration, studies on the physical mechanism of thermocapillary droplet migration under reduced gravity become more and more important. To generate the non-uniform surface tension, two different thermal sources are transmitted directly or indirectly through the bulk liquid to the droplet surface. On one hand, a vertical temperature gradient is added in the bulk liquid through providing the non-uniform temperature distribution along the interface. Young *et al.* (YGB)¹ studied thermocapillary migration of a droplet in a vertical temperature gradient field and obtained the droplet migration velocity in zero limits of Reynolds (Re) and Marangoni (Ma) numbers. Subramanian² introduced the quasi-steady-state assumption, extended the YGB results to

the small Ma numbers, and determined an asymptotic solution for the steady migration velocity. Due to effects of inertia, Bratukhin,³ Balasubramanian and Chai,⁴ and Haj-Hariri *et al.*⁵ analyzed the deformation of droplet in thermocapillary migration and found an ellipsoidal shape with the axis of rotation in the flow direction and the amplitude mainly depending on the Weber (We) number. At small We numbers, the droplet deformation in the thermocapillary droplet migration can be ignored. Since then, with the aid of the vertical temperature gradient in the bulk liquid, the thermocapillary droplet migration and its mechanism are understood very well in a series of theoretical analyses, numerical simulations, and experimental investigations.^{6–15} On the other hand, the thermal radiation to the droplet surface is another method to provide the non-uniform temperature distribution along the interface. Oliver and DeWitt (OD)¹⁶ analyzed the thermocapillary droplet migration under the thermal radiation with a uniform thermal flux at zero limits of Re and Ma numbers and

obtained the droplet migration velocity. Rednikov and Ryazantsev¹⁷ independently derived the same results and determined the deformation of the droplet. Lopez *et al.*¹⁸ and Rendondo *et al.*¹⁹ experimentally investigated thermocapillary migration of a droplet caused by laser beam heating, which makes a strongly nonhomogeneous distribution of temperature inside the droplet as well as at its surface due to the radiation absorption, and found the accelerating and steady migration processes. Ryazantsev *et al.*²⁰ reported thermo- and soluto-capillary migration of passive and active droplets with a laser beam and realized the processes of pushing, pulling, or holding stationary a droplet under various forms of illumination. Zhang *et al.*²¹ numerically studied the spontaneous droplet migration under thermal radiation with a uniform thermal flux at moderate Re numbers and determined effects of the physical parameters of two-phase fluids on the steady migration velocity. Gao and Wu²² extended the OD results under the thermal radiation to the small Re numbers, obtained an asymptotic solution for the steady migration velocity, and numerically found the linear rises of the steady-state temperatures of the two-phase fluids with time as the main feature of temperature fields during the steady migration processes.

Recently, in view of the mechanism of the varied surface tension with temperature, some topics on applications of thermocapillary droplet migration are concerned. In the fluid-handling microtechnology, it was required to form, convey, and manipulate droplets in microchannels. Originated from the interface, thermocapillary flows are particularly suitable to drive flows at small scales where surface effects dominate bulk behaviors. In some cases, the effects of gravity in a horizontal microfluidic channel are approximately omitted or removed by the density matching of two liquids. One application of thermocapillary droplet migration in a microfluidic channel is to manipulate directly a droplet with a laser beam^{23,24} or to manipulate indirectly a droplet on an absorbing substrate with a laser beam²⁵ or to manipulate a droplet with a heater.²⁶ The correspondent physical mechanism on the heating measure for the different application to generate the varied surface tension is the adding a thermal radiation flux on the interface of droplet or the setting up a temperature gradient field on the substrate.^{27,28} In comparison with the absorbing substrate and the heater driving measures, laser actuation as an attractive approach to induce thermocapillary flows has two main advantages: on one hand, the light field interactions are contactless and dynamically reconfigurable; on the other hand, the thermocapillary force generated by absorption is far stronger than the optical force, which may be ignored.^{29,30} Rybalko *et al.*³¹ reported that the directed motion of an oil droplet floating in an aqueous solution guided by a laser beam focused at the oil–water interface, where exists the variation of surface tension due to the thermal gradient. Baroud *et al.*³² shown that localized heating from a laser can block the motion of a water-in-oil droplet interface in a microchannel to act as a microfluidic valve for two-phase flows. Vincent and Delville³³ experimentally investigated thermocapillary droplet migration induced by local laser heating of the advancing front of a growing droplet confined in a microfluidic channel and realized the control of droplet size. Song *et al.*³⁴ reported the response of an oil droplet floating in an aqueous solution to local laser heating and observed distinct dynamic transitions of the shape and motion of the droplet depending on the laser power.

Moreover, although the laser radiation and the thermal radiation have different wavelengths, they have similar functions to manipulate

droplets due to the absorption of heat and the generation of capillary forces. Bezuglyi and Ivanova³⁵ and Ivanova and Bezuglyi³⁶ experimentally investigated droplet growth occurring in the layers of water-alcohol solutions under the action of laser radiation and found that the concentration-capillary mechanism enables to effectively control the rate of droplet formation. Shukla and Sallam³⁷ studied effects of liquid transparency on laser-induced motion of droplets and found that the motion of the opaque droplets was dominated by thermal Marangoni effect due to direct heating by the laser beam. Tatosova *et al.*³⁸ experimentally and numerically studied the droplet formation mechanism in thin layers of water–isopropanol mixtures under the laser heating and found that an increase in the initial concentration of isopropanol in mixture leads to a decrease in the droplet growth rate at a given power of the laser beam. In the microgravity environment, the action of laser radiation may be taken as the thermal radiation technology to control the thermocapillary droplet migration in the vertical temperature gradient field. At large Ma numbers, thermocapillary droplet migration in the vertical temperature gradient field was determined as an unsteady process, since a nonconservative integral thermal flux across the interface in the steady migration process was identified.³⁹ By adding the thermal radiation on the droplet/a thermal source in the droplet, Wu^{40,41} theoretically shown the conservative integral thermal flux across the interface in the steady thermocapillary migration process of a droplet in the vertical temperature gradient field at large Ma numbers and determined that the steady migration velocity increases with the increasing of Ma number. However, some interesting topics on thermocapillary droplet migration in the vertical temperature gradient controlled by thermal radiations at small and moderate Ma numbers, such as effects of uniform and non-uniform thermal radiations, effects of the radiation intensity on the steady migration velocity, evolutions of steady temperature distributions in the two-phase fluids referring to the different fluidic parameters remain to be studied with respect to their physical mechanisms.

In this paper, we first show analytical results of thermocapillary droplet migration in a vertical temperature gradient field controlled by thermal radiations with uniform and non-uniform thermal fluxes at zero limits of Re and Ma numbers and determine the dependence of the steady migration velocity on thermal radiation (Tr) number. Then, we numerically investigate effects of Tr number, volume heat capacity ratio, and uniform/non-uniform thermal radiation on thermocapillary droplet migration in the combined vertical temperature gradient and the thermal radiation at moderate Ma numbers. Section II describes the model and formulation of thermocapillary droplet migration in the combined vertical temperature gradient and thermal radiation. The analytical results of the steady thermocapillary migration of a droplet at zero limits of Re and Ma numbers in relation to Tr number are determined in Sec. III. The numerical results of thermocapillary droplet migration at moderate Ma and moderate Tr numbers are analyzed in Sec. IV. Finally, in Sec. V, conclusions and discussions are given.

II. MODEL AND GOVERNING EQUATIONS

Consider a single droplet with a radius R_0 (cm) placed in a continuous-phase fluid of unbounded extend under a uniform vertical temperature gradient G (K/cm) and a thermal radiation flux Ω (W/cm²), as illustrated in Fig. 1(a). Gravity is ignored. The droplet surface and the continuous-phase fluid are assumed as a gray body

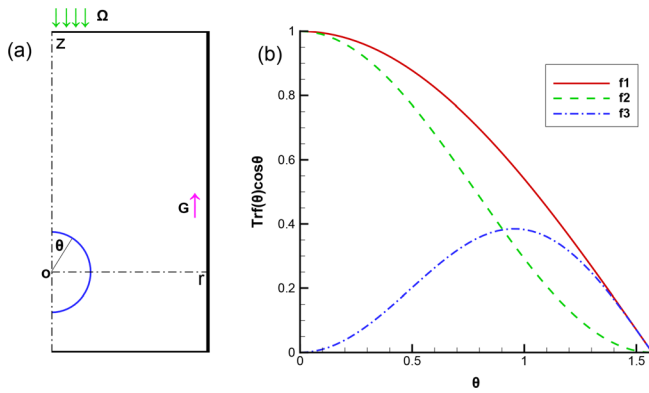


FIG. 1. (a) A schematic of the thermocapillary droplet migration system under a vertical temperature gradient G and a thermal radiation flux Ω ; (b) heat fluxes $Trf(\theta) \cos \theta$ absorbed by the upper interface of the droplet vs $\theta \in [0, \pi/2]$ for the uniform and the non-uniform thermal radiations [$f_1 = 1$, $f_2 = \cos \theta$, and $f_3 = \sin^2 \theta$] at $Tr = 1$.

and transparent to radiation, respectively. The droplet moves up due to the non-uniform surface tension $\sigma = \sigma_0 + \sigma_T(\bar{T} - T_0)$, where σ_0 (dyn/cm) and σ_T (dyn/cmK) are the surface tension coefficient at the undisturbed temperature T_0 (K) and the changing rate of the interfacial tension between the droplet and the continuous-phase fluid with temperature \bar{T} (K), respectively. The continuity, momentum, and energy equations for the continuous-phase fluid and the droplet in a laboratory coordinate system [\bar{r} (cm), \bar{z} (cm)] are written as

$$\begin{aligned} \frac{\partial \rho_i}{\partial t} + \bar{\nabla} \cdot (\rho_i \bar{\mathbf{v}}_i) &= 0, \\ \frac{\partial \rho_i \bar{\mathbf{v}}_i}{\partial t} + \bar{\nabla} \cdot (\rho_i \bar{\mathbf{v}}_i \bar{\mathbf{v}}_i) &= -\bar{\nabla} \bar{p}_i + \bar{\nabla} \cdot [\mu_i (\bar{\nabla} \bar{\mathbf{v}}_i + \bar{\nabla}^T \bar{\mathbf{v}}_i)], \\ \frac{\partial \bar{T}_i}{\partial t} + \bar{\nabla} \cdot (\bar{\mathbf{v}}_i \bar{T}_i) &= \frac{\kappa_i}{k_i} \bar{\nabla} \cdot (k_i \bar{\nabla} \bar{T}_i), \end{aligned} \quad (1)$$

where the symbols $\bar{\mathbf{v}}_i$ (cm/s), \bar{p}_i (dyn/cm²), \bar{T}_i (K) represent the velocity, pressure and temperature, respectively. The direction of the incident irradiation is antiparallel to the \bar{z} -axis. ρ_i (g/cm³), μ_i (dyns/cm²), k_i (W/cmK), and κ_i (cm²/s) represent the density, the dynamical viscosity, the thermal conductivity, and the thermal diffusivity, respectively. Symbols with subscript 1 and 2 denote physical variables and coefficients of the continuous-phase fluid and the droplet, respectively. The solutions of Eq. (1) have to satisfy the boundary conditions at infinity

$$\bar{\mathbf{v}}_1 \rightarrow 0, \quad \bar{p}_1 \rightarrow p_\infty, \quad \bar{T}_1 \rightarrow T_0 + G\bar{z} \quad (2)$$

and at the interface $\bar{\mathbf{r}}_b$ (cm) of the two-phase fluids

$$\begin{aligned} \bar{\mathbf{v}}_1(\bar{\mathbf{r}}_b, t) &= \bar{\mathbf{v}}_2(\bar{\mathbf{r}}_b, t), \\ \mathbf{n} \cdot \bar{\mathbf{\Pi}}_1 \cdot \mathbf{n} - \mathbf{n} \cdot \bar{\mathbf{\Pi}}_2 \cdot \mathbf{n} &= 2\sigma H, \\ \mathbf{n} \cdot \bar{\mathbf{\Pi}}_1 \cdot \mathbf{s} - \mathbf{n} \cdot \bar{\mathbf{\Pi}}_2 \cdot \mathbf{s} &= -\bar{\nabla}_s \sigma \cdot \mathbf{s}, \\ \bar{T}_1(\bar{\mathbf{r}}_b, t) &= \bar{T}_2(\bar{\mathbf{r}}_b, t), \\ k_1 \frac{\partial \bar{T}_1}{\partial n}(\bar{\mathbf{r}}_b, t) + \Omega \mathbf{i}_z \cdot \mathbf{n} &= k_2 \frac{\partial \bar{T}_2}{\partial n}(\bar{\mathbf{r}}_b, t), \end{aligned} \quad (3)$$

where $\bar{\mathbf{\Pi}}_1$ (dyn/cm²) and $\bar{\mathbf{\Pi}}_2$ (dyn/cm²) are the stress tensors of the two-phase fluids. \mathbf{n} and \mathbf{s} are the unit vectors normal and tangent to the interface, respectively. \mathbf{i}_z is a unit vector of the \bar{z} -axis.

$\bar{\nabla}_s (= \bar{\nabla} - \mathbf{n} \frac{\partial}{\partial n})$ is the surface gradient operator. H (cm⁻¹) is the curvature of the interface. The thermal radiation flux $\Omega [= \Theta f(\bar{\mathbf{r}}_b)]$ is assumed as a uniform or a wave function with the amplitude Θ (W/cm²).

In the modeling assumptions, both fluids are immiscible, and the physical properties are constant. The droplet keeps a spherical axisymmetric shape without deformation ($H = 1/R_0$). The equations of states for density, viscosity, heat conduction, and heat diffusivity are written as follows:

$$\frac{d\rho_i}{dt} = \frac{d\mu_i}{dt} = \frac{dk_i}{dt} = \frac{d\kappa_i}{dt} = 0. \quad (4)$$

By taking the radius of the droplet R_0 , the velocity $v_0 = -\sigma_T GR_0/\mu_1$ and GR_0 as the reference quantities to make coordinates, velocity, and temperature dimensionless, Eq. (1) is rewritten as

$$\begin{aligned} \bar{\nabla} \cdot \bar{\mathbf{v}}_i &= 0, \\ \rho_i \frac{\partial \bar{\mathbf{v}}_i}{\partial t} + \rho_i \bar{\mathbf{v}}_i \cdot \bar{\nabla} \bar{\mathbf{v}}_i &= -\bar{\nabla} \bar{p}_i + \frac{1}{Re} \bar{\nabla} \cdot [\mu_i (\bar{\nabla} \bar{\mathbf{v}}_i + \bar{\nabla}^T \bar{\mathbf{v}}_i)], \\ \frac{\partial \bar{T}_i}{\partial t} + \bar{\mathbf{v}}_i \cdot \bar{\nabla} \bar{T}_i &= \frac{\kappa_i/k_i}{Ma} \bar{\nabla} \cdot (k_i \bar{\nabla} \bar{T}_i). \end{aligned} \quad (5)$$

The physical coefficients (density ρ_i , dynamic viscosity μ_i , thermal conductivity k_i , and thermal diffusivity κ_i) are non-dimensionalized by the quantities of continuous-phase fluid. Re , Ma , Prandtl (Pr), and Tr numbers are, respectively, defined as

$$Re = \frac{\rho_1 v_0 R_0}{\mu_1}, \quad Ma = \frac{v_0 R_0}{\kappa_1}, \quad Pr = \frac{Ma}{Re} = \frac{\mu_1}{\rho_1 \kappa_1}, \quad \text{and} \quad Tr = \frac{\Theta}{G k_1}. \quad (6)$$

The solutions of Eq. (5) must satisfy the boundary conditions at infinity

$$\bar{\mathbf{v}}_1 \rightarrow 0, \quad \bar{p}_1 \rightarrow 0, \quad \bar{T}_1 \rightarrow \bar{z}, \quad (7)$$

and at the interface $\bar{\mathbf{r}}_b$ of the two-phase fluids

$$\begin{aligned} \bar{\mathbf{v}}_1(\bar{\mathbf{r}}_b, t) &= \bar{\mathbf{v}}_2(\bar{\mathbf{r}}_b, t), \\ \mathbf{n} \cdot \bar{\mathbf{\Pi}}_1 \cdot \mathbf{n} - \mathbf{n} \cdot \bar{\mathbf{\Pi}}_2 \cdot \mathbf{n} &= \frac{2}{Re} \sigma H, \\ \mathbf{n} \cdot \bar{\mathbf{\Pi}}_1 \cdot \mathbf{s} - \mathbf{n} \cdot \bar{\mathbf{\Pi}}_2 \cdot \mathbf{s} &= -\frac{1}{Re} \frac{\partial \sigma}{\partial s}, \\ \bar{T}_1(\bar{\mathbf{r}}_b, t) &= \bar{T}_2(\bar{\mathbf{r}}_b, t), \\ \frac{\partial \bar{T}_1}{\partial n}(\bar{\mathbf{r}}_b, t) + Trf(\bar{\mathbf{r}}_b) \mathbf{i}_z \cdot \mathbf{n} &= k_2 \frac{\partial \bar{T}_2}{\partial n}(\bar{\mathbf{r}}_b, t), \end{aligned} \quad (8)$$

where $\sigma = \frac{1}{Ca} - \bar{T}_1$. $Ca (= \frac{v_0 \mu}{\sigma_0})$ is the Capillary number.

III. THEORETICAL ANALYSIS OF THERMOCAPILLARY DROPLET MIGRATION AT ZERO LIMITS OF Re AND Ma NUMBERS

At zero limits of Re and Ma numbers, the momentum and energy equations in Eq. (5) are written in a spherical coordinate system (r, θ) moving with the droplet

$$\begin{aligned} \Delta \mathbf{v}_i &= 0 \quad \text{or} \quad E^4 \psi_i = 0, \\ \Delta T_i &= 0, \end{aligned} \quad (9)$$

where

$$E^2 = \frac{\partial^2}{\partial r^2} + \frac{\sin^2 \theta}{r^2} \frac{\partial^2}{\partial (\cos \theta)^2}, \quad (10)$$

and ψ_i is the stream functions of the continuous fluid and the droplet. At the place far from the droplet, the velocity and temperature of the continuous-phase fluid should satisfy

$$\begin{aligned} \mathbf{v}_1(r \rightarrow \infty, \theta) &\rightarrow (-V_\infty \cos \theta, V_\infty \sin \theta), \\ T_1(r \rightarrow \infty, \theta) &\rightarrow r \cos \theta. \end{aligned} \quad (11)$$

At the droplet surface, the velocities inside and outside the droplet must meet the continuous and impermeable conditions described below

$$\begin{aligned} v_{r,1}(1, \theta) = v_{r,2}(1, \theta) &= 0, \\ v_{\theta,1}(1, \theta) = v_{\theta,2}(1, \theta). \end{aligned} \quad (12)$$

Meanwhile, the temperatures and the heat fluxes inside and outside the droplet must be continuous and in balance with the thermal radiation as given below, respectively,

$$T_1(1, \theta) = T_2(1, \theta) \quad (13)$$

and

$$\begin{aligned} \frac{\partial T_1}{\partial r}(1, \theta) + Trf(\theta) \cos \theta &= k_2 \frac{\partial T_2}{\partial r}(1, \theta), \quad \theta \in [0, \pi/2], \\ \frac{\partial T_1}{\partial r}(1, \theta) &= k_2 \frac{\partial T_2}{\partial r}(1, \theta), \quad \theta \in [\pi/2, \pi]. \end{aligned} \quad (14)$$

The difference of the tangential stresses is balanced by the interfacial gradient of the surface tension

$$\Pi_{r\theta,1}(1, \theta) - \Pi_{r\theta,2}(1, \theta) = \frac{1}{Re} \frac{\partial T_1}{\partial \theta}(1, \theta), \quad (15)$$

where $\Pi_{r\theta,i} = \frac{\mu_i}{Re} [r \frac{\partial}{\partial r} (\frac{v_{\theta,i}}{r}) + \frac{1}{r} \frac{\partial v_{r,i}}{\partial \theta}]$.

A. Uniform thermal radiation [$f_1(\theta) = 1$]

Following the methods for solving the problems for low Reynolds number hydrodynamics,^{16,42,43} the solutions of the governing equation (9) satisfying the boundary conditions (11)–(15) with the uniform thermal radiation [$f_1(\theta) = 1$] can be determined as

$$\begin{aligned} \psi_1 &= \frac{V_\infty}{2} (r^2 - r^{-1}) \sin^2 \theta \\ &+ \sum_{n=3, \text{odd}}^\infty D_n (r^{3-n} - r^{1-n}) C_n^{-1/2}(\cos \theta), \\ \psi_2 &= \frac{3V_\infty}{4} (r^4 - r^2) \sin^2 \theta \\ &+ \sum_{n=3, \text{odd}}^\infty D_n (r^{2+n} - r^n) C_n^{-1/2}(\cos \theta) \end{aligned} \quad (16)$$

and

$$\begin{aligned} T_1 &= \frac{Tr}{4} r^{-1} + \left[r + \frac{2 - 2k_2 + Tr}{2(2 + k_2)} r^{-2} \right] \cos \theta \\ &+ \sum_{n=2, \text{even}}^\infty a_n r^{-(n+1)} P_n(\cos \theta), \\ T_2 &= \frac{Tr}{4} + \frac{6 + Tr}{2(2 + k_2)} r \cos \theta + \sum_{n=2, \text{even}}^\infty a_n r^n P_n(\cos \theta), \end{aligned} \quad (17)$$

where $a_n = (-1)^{(n-2)/2} \frac{(2n+1)Tr}{2[(1+k_2)n+1](n+2)(n-1)} \prod_{j=1}^{n/2} \frac{2j-1}{2j}$, ($n \geq 2$, even), $D_n = \frac{n(n-1)}{2(2n-1)(1+\mu_2)} a_{n-1}$, ($n \geq 3$, odd). $P_n(s)$ and $C_n^{-1/2}(s) = \int_s^1 P_{n-1}(x) dx$ are the Legendre and Gegenbauer polynomials of order n , respectively. The steady migration velocity is obtained through the net force balance condition and written as

$$V_{1,\infty} = \frac{6 + Tr}{3(2 + 3\mu_2)(2 + k_2)}. \quad (18)$$

It is noted that the migration velocity $V_{1,\infty}$ returns to the original one for thermocapillary droplet migration in the vertical temperature gradient field, when Tr number is zero. Under the control of the uniform thermal radiation, the migration velocity $V_{1,\infty}$ raises as Tr number increases.

B. Non-uniform thermal radiation [$f_2(\theta) = \cos \theta$]

Using the above methods, the solutions of the governing equation (9) satisfying the boundary conditions (11)–(15) with the non-uniform thermal radiation [$f_2(\theta) = \cos \theta$] can be determined as

$$\begin{aligned} \psi_1 &= \frac{V_\infty}{2} (r^2 - r^{-1}) \sin^2 \theta \\ &+ \frac{Tr}{5(3 + 2k_2)(1 + \mu_2)} (1 - r^{-2}) C_3^{-1/2}(\cos \theta) \\ &+ \sum_{n=4, \text{even}}^\infty D_n (r^{3-n} - r^{1-n}) C_n^{-1/2}(\cos \theta), \\ \psi_2 &= \frac{3V_\infty}{4} (r^4 - r^2) \sin^2 \theta \\ &+ \frac{Tr}{5(3 + 2k_2)(1 + \mu_2)} (r^5 - r^3) C_3^{-1/2}(\cos \theta) \\ &+ \sum_{n=4, \text{even}}^\infty D_n (r^{2+n} - r^n) C_n^{-1/2}(\cos \theta), \end{aligned} \quad (19)$$

and

$$\begin{aligned} T_1 &= \frac{Tr}{6} r^{-1} + \left[r + \frac{8 - 8k_2 + 3Tr}{8(2 + k_2)} r^{-2} \right] \cos \theta \\ &+ \frac{Tr}{3(3 + 2k_2)} r^{-3} P_2(\cos \theta) \\ &+ \sum_{n=3, \text{odd}}^\infty a_n r^{-(n+1)} P_n(\cos \theta), \\ T_2 &= \frac{Tr}{6} + \frac{3(8 + Tr)}{8(2 + k_2)} r \cos \theta + \frac{Tr}{3(3 + 2k_2)} r^2 P_2(\cos \theta) \\ &+ \sum_{n=3, \text{odd}}^\infty a_n r^n P_n(\cos \theta), \end{aligned} \quad (20)$$

where $a_n = (-1)^{(n+1)/2} \frac{(2n+1)Tr}{[(1+k_2)n+1](n-2)(n+1)(n+3)} \prod_{j=1}^{(n-1)/2} \frac{2j-1}{2j}$, ($n \geq 3$, odd), $D_n = \frac{n(n-1)}{2(2n-1)(1+\mu_2)} a_{n-1}$, ($n \geq 4$, even). The steady migration velocity is obtained through the net force balance condition and written as

$$V_{2,\infty} = \frac{8 + Tr}{4(2 + 3\mu_2)(2 + k_2)}. \quad (21)$$

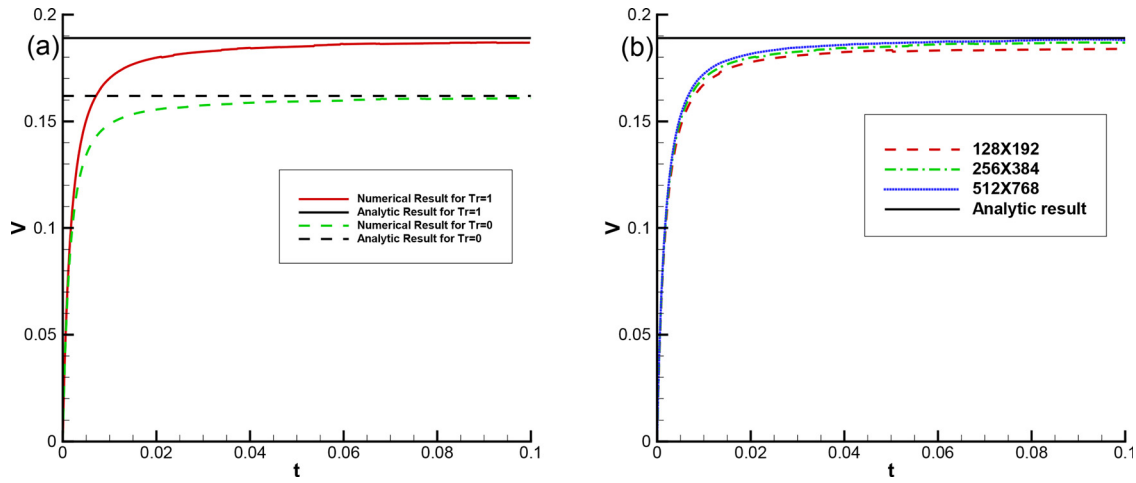


FIG. 2. Droplet migration velocity vs non-dimensional time (a) for $Tr = 1$ (the combined YGB¹ and OD¹⁶ model) and 0 (the YGB model) with the grid resolution 256×384 ; (b) for $Tr = 1$ with three grid resolutions 128×192 , 256×384 , and 512×768 at $Re = Ma = 0.01$, $Ca = 0.1$, and $\rho_2 = \mu_2 = k_2 = \kappa_2 = 0.8$. The correspondent analytical results at zero limits of Re and Ma numbers are also provided for comparison.

It is noted that the migration velocity $V_{2,\infty}$ returns to the original one for thermocapillary droplet migration in the vertical temperature gradient field, when Tr number is zero. Under the action of the non-uniform thermal radiation with $f_2(\theta) = \cos \theta$, the migration velocity $V_{2,\infty}$ raises as Tr number increases. In comparison with the uniform thermal radiation [$f_1(\theta) = 1$], at a fixed Tr number, the migration velocity $V_{2,\infty}$ is smaller than $V_{1,\infty}$.

C. Non-uniform thermal radiation [$f_3(\theta) = \sin^2 \theta$]

The non-uniform thermal radiation with $f_3(\theta) = \sin^2 \theta$ was used to investigate the steady thermocapillary droplet migration at large Ma numbers under the vertical temperature gradient and the non-

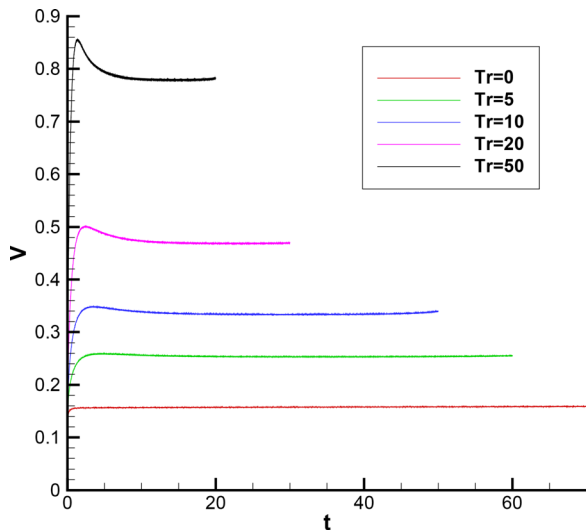


FIG. 3. Time evolutions of droplet migration velocities for $Tr = 0, 5, 10, 20$, and 50 at the fixed $Ma = 5$, $Pr = 50$, $Ca = 0.1$, and $\rho_2 = \mu_2 = k_2 = \kappa_2 = 0.8$.

uniform thermal radiation.⁴⁰ Following the above derivations, the solutions of the governing equation (9) satisfying the boundary conditions (11)–(15) with the non-uniform thermal radiation [$f_3(\theta) = \sin^2 \theta$] can be determined as

$$\begin{aligned} \psi_1 &= \frac{V_\infty}{2} (r^2 - r^{-1}) \sin^2 \theta \\ &\quad - \frac{6Tr}{35(4 + 3k_2)(1 + \mu_2)} (r^{-1} - r^{-3}) C_4^{-1/2}(\cos \theta) \\ &\quad + \sum_{n=5, odd}^\infty D_n (r^{3-n} - r^{1-n}) C_n^{-1/2}(\cos \theta), \\ \psi_2 &= \frac{3V_\infty}{4} (r^4 - r^2) \sin^2 \theta \\ &\quad - \frac{6Tr}{35(4 + 3k_2)(1 + \mu_2)} (r^6 - r^4) C_4^{-1/2}(\cos \theta) \\ &\quad + \sum_{n=5, odd}^\infty D_n (r^{2+n} - r^n) C_n^{-1/2}(\cos \theta), \end{aligned} \tag{22}$$

and

$$\begin{aligned} T_1 &= \frac{3Tr}{40} r^{-1} + \left[r + \frac{5 - 5k_2 + Tr}{5(2 + k_2)} r^{-2} \right] \cos \theta \\ &\quad - \frac{Tr}{5(4 + 3k_2)} r^{-4} P_3(\cos \theta) \\ &\quad + \sum_{n=4, even}^\infty a_n r^{-(n+1)} P_n(\cos \theta), \\ T_2 &= \frac{3Tr}{40} + \frac{15 + Tr}{5(2 + k_2)} r \cos \theta - \frac{Tr}{5(4 + 3k_2)} r^3 P_3(\cos \theta) \\ &\quad + \sum_{n=4, even}^\infty a_n r^n P_n(\cos \theta), \end{aligned} \tag{23}$$

where $a_n = (-1)^{n/2} \frac{(2-n)(3+n)(2n+1)Tr}{2[(1+k_2)n+1](n-1)(n-3)(n+2)(n+4)} \prod_{j=1}^{n/2} \frac{2j-1}{2j}$, ($n \geq 4$, even), $D_n = \frac{n(n-1)}{2(2n-1)(1+\mu_2)} a_{n-1}$, ($n \geq 5$, odd). The steady migration

velocity is obtained through the net force balance condition and written as

$$V_{3,\infty} = \frac{2(15 + Tr)}{15(2 + 3\mu_2)(2 + k_2)}. \quad (24)$$

It is noted that the migration velocity $V_{3,\infty}$ returns to the original one for thermocapillary droplet migration in the vertical temperature gradient field, when Tr number is zero. Under the non-uniform thermal radiation with $f_3(\theta) = \sin^2\theta$, the migration velocity $V_{3,\infty}$ raises as Tr number increases. In comparison with the uniform thermal radiation [$f_1(\theta) = 1$] and the non-uniform thermal radiation [$f_2(\theta) = \cos\theta$], at a fixed Tr number, the migration velocity $V_{3,\infty}$ is smaller than $V_{1,\infty}$ and $V_{2,\infty}$.

As given in Eq. (14), the droplet obtains the additional thermal energy via the heat flux $Trf(\theta)\cos\theta$ across the interface provided by the thermal radiation. For the uniform and non-uniform thermal radiations [$f_1(\theta) = 1$, $f_2(\theta) = \cos\theta$, and $f_3(\theta) = \sin^2\theta$], the heat fluxes $Trf(\theta)\cos\theta$ absorbed by the upper interface of the droplet vs $\theta \in [0, \pi/2]$ at $Tr = 1$ are shown in Fig. 1(b). It reveals that the integral heat fluxes at the upper interface, that is, the areas surrounded by the curves and the one/two coordinate axes, for the uniform and non-uniform thermal radiations have the following relationship:

$$\begin{aligned} \int_0^{\pi/2} Trf_1(\theta)\cos\theta d\theta &> \int_0^{\pi/2} Trf_2(\theta)\cos\theta d\theta \\ &> \int_0^{\pi/2} Trf_3(\theta)\cos\theta d\theta > 0, \end{aligned} \quad (25)$$

which corresponds to the above result for the migration velocities, that is,

$$V_{1,\infty} > V_{2,\infty} > V_{3,\infty}. \quad (26)$$

Moreover, under the vertical temperature gradient field, the change of the heat flux $Trf(\theta)\cos\theta$ absorbed by the upper interface with θ provides the additional tangential surface tension in $\frac{\partial T_i}{\partial \theta}(1, \theta)$. As given in Eq. (15), to satisfy the shear stress boundary condition, the variational tangential surface tensions $\frac{\partial T_i}{\partial \theta}(1, \theta)$ for the uniform and non-uniform thermal radiations [$f_1(\theta) = 1$, $f_2(\theta) = \cos\theta$, and $f_3(\theta) = \sin^2\theta$] cause different shear stresses of the continuous-phase fluid and the droplet, that is, different velocity fields in Eqs. (16), (19), and (22).

IV. NUMERICAL SIMULATION OF THERMOCAPILLARY DROPLET MIGRATION AT MODERATE Ma AND MODERATE Tr NUMBERS

A. Numerical methods

As shown schematically in Fig. 1(a), the symmetric axis of the container is taken as the \bar{z} -axis. An axisymmetric droplet is placed

initially at the center of coordinates and then moved along the \bar{z} -axis under a vertical temperature gradient and a uniform/non-uniform thermal radiation flux. The continuous, momentum, and energy equations with the surface tension force δF_σ and the radiative heat energy δQ in a cylindrical coordinate system $\bar{\mathbf{r}} = (\bar{r}, \bar{z})$ are written as

$$\begin{aligned} \bar{\nabla} \cdot \bar{\mathbf{v}}_i &= 0, \\ \frac{\partial(\rho_i \bar{\mathbf{v}}_i)}{\partial t} + \bar{\nabla} \cdot (\rho_i \bar{\mathbf{v}}_i \bar{\mathbf{v}}_i) &= -\bar{\nabla} \bar{p}_i + \frac{1}{Re} \bar{\nabla} \cdot [\mu_i (\bar{\nabla} \bar{\mathbf{v}}_i + \bar{\nabla} \bar{\mathbf{v}}_i^T)] \\ &\quad + \frac{1}{Re} \delta \mathbf{F}_\sigma, \end{aligned} \quad (27)$$

$$\frac{\partial \bar{T}_i}{\partial t} + \bar{\mathbf{v}}_i \cdot \bar{\nabla} \bar{T}_i = \frac{\kappa_i/k_i}{Ma} \bar{\nabla} \cdot (k_i \bar{\nabla} \bar{T}_i) + \frac{\kappa_i/k_i}{Ma} \delta Q,$$

where

$$\begin{aligned} \delta \mathbf{F}_\sigma &= \frac{\int_{\Delta s_{AB}} \left(-2\sigma H \mathbf{n} + \frac{\partial \sigma}{\partial s} \mathbf{s} \right) 2\pi r \delta^2(\bar{\mathbf{r}} - \bar{\mathbf{r}}_b) ds}{2\pi r_c \Delta r \Delta z} \\ &= \frac{[(\sigma r s)_B - (\sigma r s)_A] - \sigma_c \Delta s_{AB} \hat{\mathbf{i}}_{\bar{r}}}{r_c \Delta r \Delta z} \end{aligned} \quad (28)$$

and

$$\begin{aligned} \delta Q &= Tr \delta q, \\ \delta q &= \frac{\int_{\Delta s_{AB}} f(\bar{\mathbf{r}}_b) (\hat{\mathbf{i}}_{\bar{z}} \cdot \mathbf{n}) 2\pi r \delta^2(\bar{\mathbf{r}} - \bar{\mathbf{r}}_b) ds}{2\pi r_c \Delta r \Delta z} \\ &= \frac{\int_{\Delta s_{AB}} f(s) (\hat{\mathbf{i}}_{\bar{z}} \cdot \mathbf{n}) (\hat{\mathbf{i}}_{\bar{r}} \cdot \mathbf{n}) ds}{r_c \Delta r \Delta z} = \frac{\int_{\Delta \theta_{AB}} f(\theta) \cos\theta \sin\theta d\theta}{r_c \Delta r \Delta z}, \end{aligned} \quad (29)$$

where δ^2 is a two-dimensional function constructed by the repeated multiplication of the one-dimensional Dirac delta function. $\hat{\mathbf{i}}_{\bar{r}}$ is a unit vector of the \bar{r} -axis. Δs_{AB} is a short front element on the interface. r_c is the radius of the cross section at the center c of Δs_{AB} . θ is the angle coordinate of the interface s as shown in Fig. 1(a). The solutions of Eq. (27) should satisfy the initial conditions of the half domain $\bar{r} \in [0, r_1]$ and $\bar{z} \in [z_1, z_2]$

$$\begin{aligned} \bar{\mathbf{v}}_i &= 0, \\ \bar{T}_i &= \bar{z} \end{aligned} \quad (30)$$

and the boundary conditions at the top and bottom walls ($\bar{z} = z_1$ and $\bar{z} = z_2$), on the central symmetric axis ($\bar{r} = 0$) and at the right wall ($\bar{r} = r_1$)

$$\begin{aligned} \bar{v}_{r,1}(\bar{r}, z_1) = \bar{v}_{r,1}(\bar{r}, z_2) = 0, \quad \frac{\partial \bar{v}_{z,1}}{\partial z}(\bar{r}, z_1) = \frac{\partial \bar{v}_{z,1}}{\partial z}(\bar{r}, z_2) = 0, \quad \bar{T}_1(\bar{r}, z_1) = z_1, \quad \bar{T}_1(\bar{r}, z_2) = z_2, \\ \bar{v}_{r,i}(0, \bar{z}) = 0, \quad \frac{\partial \bar{v}_{z,i}}{\partial r}(0, \bar{z}) = 0, \quad \frac{\partial \bar{T}_i}{\partial r}(0, \bar{z}) = 0, \\ \bar{v}_{r,1}(r_1, \bar{z}) = 0, \quad \frac{\partial \bar{v}_{z,1}}{\partial r}(r_1, \bar{z}) = 0, \quad \bar{T}_1(r_1, \bar{z}) = \bar{z}. \end{aligned} \quad (31)$$

In the following computation, we apply a fixed regular staggered Marker-and-Cell grid in the computational domain, a second-order central difference scheme for the spatial variables, and an explicit predictor–corrector second-order scheme for time integration of the above momentum and energy equations. Since both fluids are assumed immiscible, all physical coefficients are discontinuous across the interface. The interface is captured and updated by the front-tracking method,⁴⁴ so all discontinuous physical coefficients across the interface are treated as continuous. The conversion of the physical quantities between the interface nodes (\bar{r}_p, \bar{z}_p) and the grid points ($i\Delta\bar{r}, j\Delta\bar{z}$) is treated with the Peskin’s weighting function⁴⁵

$$w_{ij}(\bar{\mathbf{r}}_p) = d(\bar{\mathbf{r}}_p - i\Delta\bar{\mathbf{r}})d(\bar{\mathbf{z}}_p - j\Delta\bar{\mathbf{z}}), \quad (32)$$

$$d(r) = \begin{cases} (1/4h)[1 + \cos(\pi r/2h)], & |r| < 2h, \\ 0, & |r| \geq 2h, \end{cases} \quad (33)$$

where h is the grid spacing in r . To calculate the surface tension force $\delta\mathbf{F}_\sigma$, the temperature on the interface is determined by interpolating values on the grid points. The tangent vector \mathbf{s} is computed from a Lagrangian interpolation polynomial fitting through four interface nodes. The surface tension force $\delta\mathbf{F}_\sigma$ and the radiative heat energy δQ on the interface are distributed to the grid points by means of the weighting function (32), respectively. More details of the numerical methods can be found in Refs. 44 and 46.

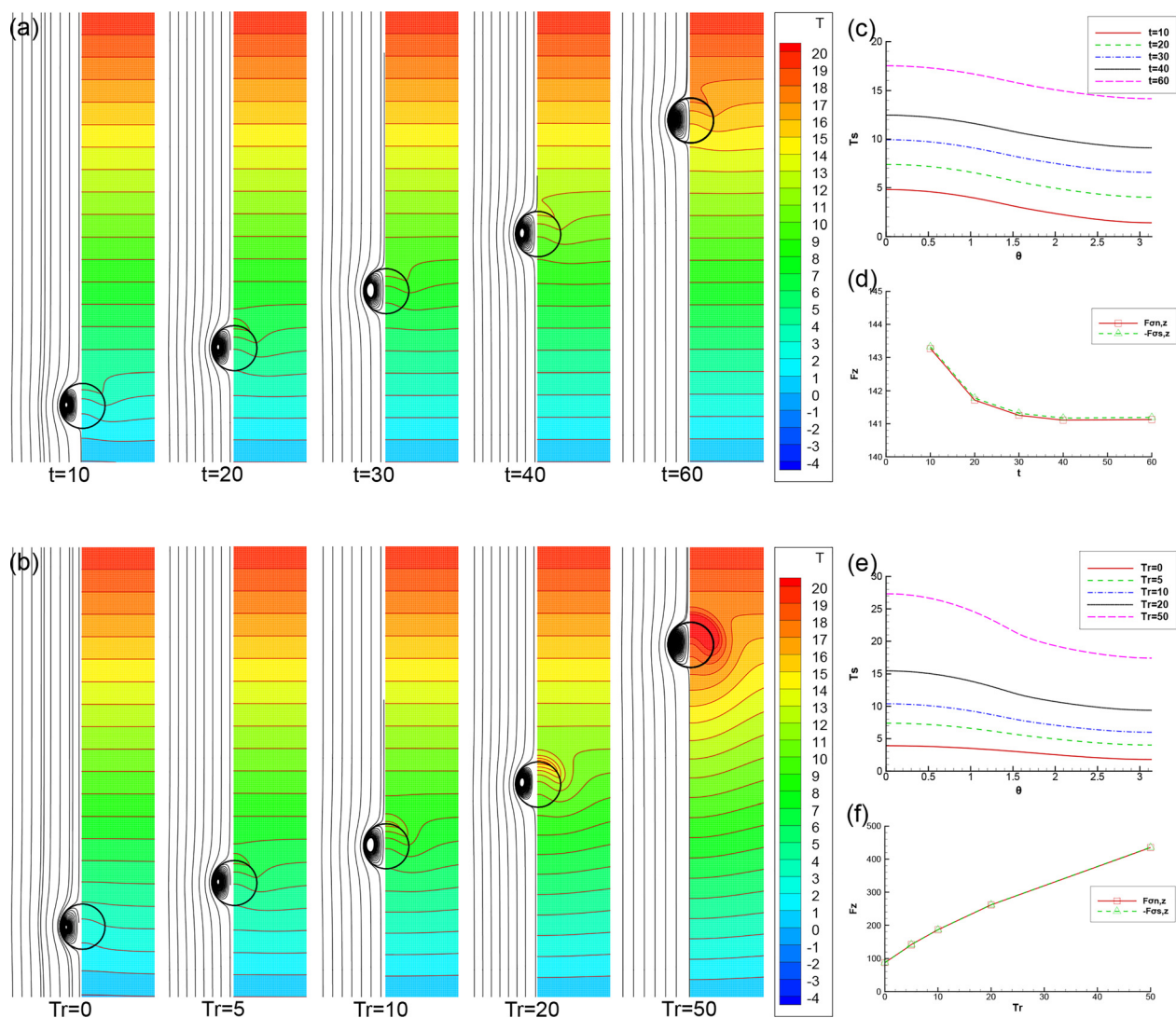


FIG. 4. Streamlines in the reference frame moving with the droplet generated by the mirror symmetry and isotherms in a laboratory coordinate frame for $Ma = 5$, $Pr = 50$, $Ca = 0.1$, and $\rho_2 = \mu_2 = k_2 = \kappa_2 = 0.8$ (a) at $t = 10, 20, 30, 40$, and 60 and the fixed $Tr = 5$; (b) at $Tr = 0, 5, 10, 20$, and 50 and the fixed $t = 20$. The correspondent interface temperature T_s vs θ and the total normal (tangential) surface force $F_{\sigma n, \bar{z}}$ ($-F_{\sigma t, \bar{z}}$) on the droplet projected to the \bar{z} direction vs t or Tr are drawn in (c) and (d) and (e) and (f), respectively.

B. Numerical results

To validate the code, we perform several calculations for the droplet migration at $Re = Ma = 0.01$, $Ca = 0.1$, and $\rho_2 = \mu_2 = k_2 = \kappa_2 = 0.8$ using the method described above. The vertical temperature gradient and the uniform thermal radiation [$f_1(\theta) = 1$] are placed, so that the radiation heat energy function in Eq. (29) is written as

$$\delta q_1 = \frac{\sin^2 \theta_B - \sin^2 \theta_A}{2r_c \Delta \bar{r} \Delta \bar{z}} \approx \frac{\sin \theta_A \cos \theta_A \Delta \theta_{AB}}{r_c \Delta \bar{r} \Delta \bar{z}}, \quad (34)$$

where $\theta_B = \theta_A + \Delta \theta_{AB}$. The computational domain is chosen as $\{\bar{r}, \bar{z}\} \in \{[0, 8], [-4, 8]\}$. First of all, we compare numerical results with analytical results at zero limits of Re and Ma numbers. The grid resolution is chosen as 256×384 grid points, that is, 32 grid points per droplet radius. As shown in Fig. 2(a), both the numerical migration velocities of the droplet at $Tr = 1$ (the combined YGB¹ and OD¹⁶ model) and $Tr = 0$ (the YGB model) exhibit convergent approximations to the above and the YGB analytical results in (18), respectively. The differences of the terminal migration velocities for $Tr = 1$ and 0 from the correspondent analytical results are very small (1.1% and 0.6%, respectively). Second, to check the sensitivity of numerical results to grid refinements, we compare numerical results for $Tr = 1$ with three grid resolutions 128×192 , 256×384 , and 512×768 (16, 32, and 64 grid points per droplet radius) with the above analytical result at zero limits of Re and Ma numbers in Fig. 2(b). The terminal migration velocity curve seems to converge toward the analytical result when the grid becomes finer. The difference in the migration velocities computed with 32 and 64 grid points per droplet radius is very small (about 1%). In the following calculations, we fix 256×384 grid points (32 grid points per droplet radius) as the grid resolution, the Pr number as 50 and the time step as 2×10^{-5} . The above other parameters are kept unless otherwise indicated.

1. Effects of Tr number on thermocapillary droplet migration

The time evolutions of the droplet migration velocities under the vertical temperature gradient and the uniform thermal radiation at $Ma = 5$ and $Tr = 0, 5, 10, 20,$ and 50 are shown in Fig. 3. For lower Tr (≤ 5) case, the droplet migration velocity first monotonically increases as time increases, and then approaches to a steady value. The transient migration process before reaching the steady state is longer as Tr number increases. The global evolution process (two stages) of the droplet migration is similar to that under a vertical temperature gradient ($Tr = 0$). For higher Tr (> 5) case, a decelerating process appears after the accelerating one; that is, a overshoot stage exists in the transient process. The overshoot amplitude raises as Tr number increases. After the overshoot stage, the droplet migration velocity approaches to a steady value. In the range of Tr number, the steady migration velocity increases as Tr number increases. Figure 4(a) displays the pattern evolution of streamlines in a reference frame moving with the droplet generated by the mirror symmetry and isotherms in a laboratory coordinate system at $Ma = 5$ and $Tr = 5$. In the migration process, when the external streamlines go around the droplet, a Hill’s spherical vortex appears within the droplet. Meanwhile, the isotherms far away from the droplet remain horizontal without disturbances. The isotherms near and inside the droplet bend to the downstream direction

along the interface and the migration direction, respectively. Since the heat flux absorbed by the interface is a cosine function, a temperature gradient along the interface generated by the thermal radiation is added. The combined interfacial temperature gradients lead to the larger non-uniform surface tension distribution. As a result, the driving force generated by the larger surface tension accelerates the droplet to move up.

To clarify the pattern evolution of the above isotherms in a laboratory coordinate system, we draw the correspondent interface temperature T_s vs θ at $t = 10, 20, 30, 40,$ and 60 in Fig. 4(c). At a fixed time, T_s monotonously decreases as θ increases. It represents the change of the normal surface tension module $|2\sigma H/Re| = |2(1/Ca - T_s)/Re|$. Meanwhile, the gradient of T_s with respect to θ causes the tangential surface tension module $|\nabla_s \sigma \cdot \mathbf{s}/Re| = |(\partial T_s / \partial \theta)/Re|$. As time increases, T_s monotonously increases but the shape of curve of T_s with θ is approximately kept. It reveals that the normal surface tension module changes with t but the tangential surface tension module approximately does not change. To quantitatively depict the changes of normal and the tangential surface tensions exerted at the interface in the migration process, we can, respectively, calculate the total normal and tangential surface forces on the droplet projected to the z direction described below

$$\begin{aligned} F_{\sigma n, z} &= \int \mathbf{f}_{\sigma n} \cdot \mathbf{i}_z 2\pi r_c ds = \frac{2\pi}{Re} \int -2\sigma H \mathbf{n} \cdot \mathbf{i}_z r_c ds \\ &= -\frac{4\pi}{Re} \int_0^\pi \sigma \cos \theta \sin \theta d\theta \\ &= -\frac{4\pi}{Re} \int_0^\pi \left(\frac{1}{Ca} - T_s\right) \cos \theta \sin \theta d\theta \\ &= \frac{4\pi}{Re} \int_0^\pi T_s \cos \theta \sin \theta d\theta, \end{aligned} \quad (35)$$

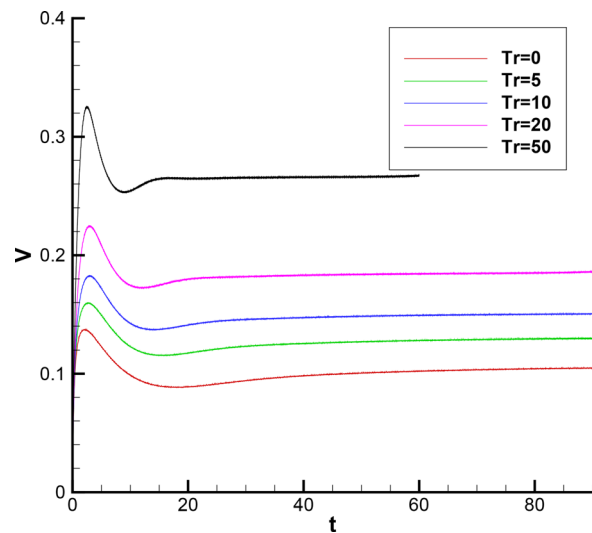


FIG. 5. Time evolutions of droplet migration velocities for $Tr = 0, 5, 10, 20,$ and 50 at the fixed $Ma = 100$, $Pr = 50$, $Ca = 0.1$ and $\rho_2 = \mu_2 = k_2 = \kappa_2 = 0.8$.

and

$$\begin{aligned}
 F_{\sigma s, \bar{z}} &= \int \mathbf{f}_{\sigma s} \cdot \mathbf{i}_{\bar{z}} 2\pi r_c ds = \frac{2\pi}{Re} \int (\nabla_s \cdot \boldsymbol{\sigma} \cdot \mathbf{s}) \cdot \mathbf{i}_{\bar{z}} r_c ds \\
 &= -\frac{2\pi}{Re} \int_0^\pi \frac{\partial \sigma}{\partial \theta} \sin^2 \theta d\theta \\
 &= \frac{2\pi}{Re} \int_0^\pi \frac{\partial T_s}{\partial \theta} \sin^2 \theta d\theta,
 \end{aligned} \tag{36}$$

where $F_{\sigma n, \bar{z}}$ and $F_{\sigma s, \bar{z}}$ are non-dimensionalized by $\rho_1 v_o^2 R_0^2$ and show them in Fig. 4(d). As time increases, the total normal surface force $F_{\sigma n, \bar{z}}$ approaches a constant. At each time, the total normal surface

force $F_{\sigma n, \bar{z}}$ and the total tangential surface force $F_{\sigma s, \bar{z}}$ are approximately opposite numbers to each other.

Figure 4(b) displays the streamlines in a reference frame moving with the droplet generated by the mirror symmetry and isotherms in a laboratory coordinate system at the steady migration state ($t = 20$) for $Ma = 5$ and $Tr = 0, 5, 10, 20,$ and 50 . In the range of Tr number, the external flow just passes around the droplet and does not separate from the droplet surface, and the Hill's spherical vortex within the droplet is kept. The computed velocity fields are thus similar. As Tr increases, a higher temperature region is formed in both fluids near the top of droplet and enlarged to be a higher temperature belt distributed near the upper hemisphere. At $Tr = 50$, the higher temperature

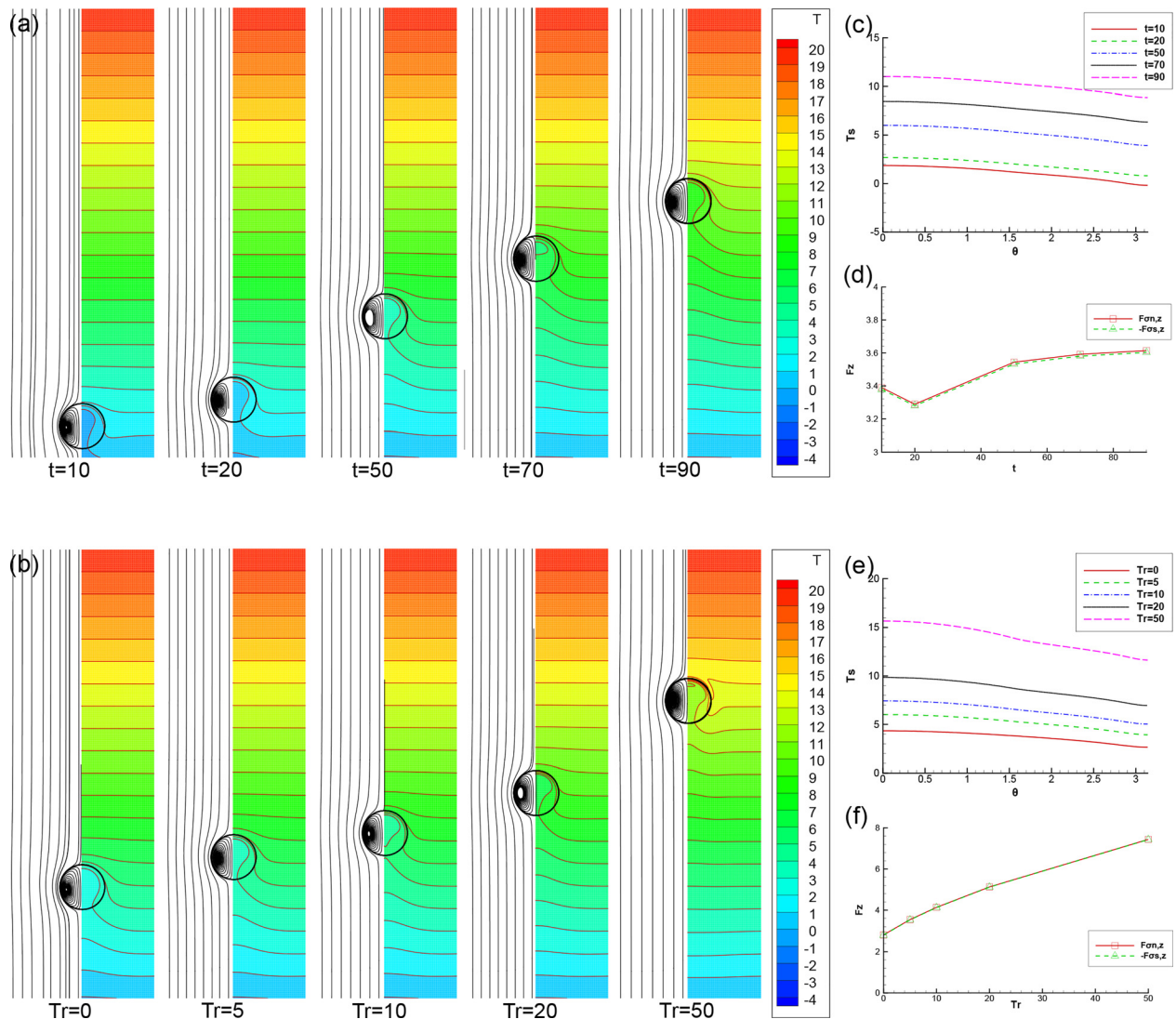


FIG. 6. Streamlines in the reference frame moving with the droplet generated by the mirror symmetry and isotherms in a laboratory coordinate frame for $Ma = 100$, $Pr = 50$, $Ca = 0.1$, and $\rho_2 = \mu_2 = k_2 = \kappa_2 = 0.8$ (a) at $t = 10, 20, 50, 70,$ and 90 and the fixed $Tr = 5$; (b) at $Tr = 0, 5, 10, 20,$ and 50 and the fixed $t = 50$. The correspondent interface temperature T_s vs θ and the total normal (tangential) surface force $F_{\sigma n, \bar{z}}$ ($-F_{\sigma s, \bar{z}}$) on the droplet projected to the \bar{z} direction vs t or Tr are drawn in (c) and (d) and (e) and (f), respectively.

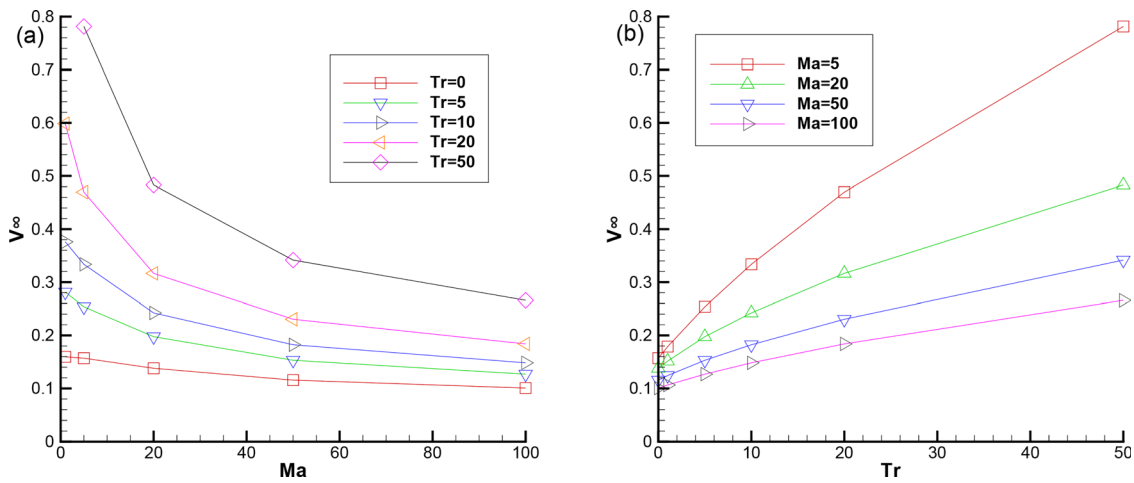


FIG. 7. (a) Steady migration velocity vs Ma number at $Tr = 0, 5, 10, 20,$ and 50 ; (b) steady migration velocity vs Tr number at $Ma = 5, 20, 50,$ and 100 .

belt spreads to the lower hemisphere, so that the isotherms in a wider range outside the droplet bend to the downstream direction. The enhanced temperature gradient along the interface induces a larger surface tension. As a result, the droplet velocity at the steady migration state ($t = 20$) increases as Tr number increases. At $Ma = 5$, the heat convection plays an equal role as the heat conduction in the energy redistribution. On one hand, the thermal energy of the interface absorbed from the thermal radiation is transferred to both fluids through the heat conduction. A local higher temperature region near the interface is formed. The higher temperature region in both fluids along the normal direction of the interface is larger as Tr number increases. On the other hand, the thermal energy of the interface is transported along the streamlines by the heat convection. The higher temperature region in both fluids along the tangent direction of the interface is enlarged as Tr number increases. As a result, the isotherms near the interface at the lower hemisphere and far from the interface bend to the downstream direction. The topological characteristics of the temperature fields in the steady migration process are very different from that in thermocapillary droplet migration with a vertical temperature gradient ($Tr = 0$). Figure 4(e) shows that as Tr increases, the interface temperature T_s monotonously increases and the absolute value of temperature gradient $|\partial T_s / \partial \theta|$ also increases. In particular, for $Tr > 0$, the growth rate of $|\partial T_s / \partial \theta|$ on the upper interface is larger than that on the lower one. It reveals that both the normal and tangential surface tension modules change with Tr . As shown in Fig. 4(f), the total normal surface force $F_{\sigma n, \bar{z}}$ monotonously increases with the increasing of Tr . At each Tr , the total normal surface force $F_{\sigma n, \bar{z}}$ and the total tangential surface force $F_{\sigma t, \bar{z}}$ are approximately opposite numbers to each other.

The time evolutions of the droplet migration velocities under the vertical temperature gradient and the uniform thermal radiation at $Ma = 100$ and $Tr = 0, 5, 10, 20,$ and 50 are shown in Fig. 5. In the range of Tr number, three stages (acceleration, deceleration, and steady) appear in the droplet migration processes. The amplitude of the overshoot stage in the transient process raises as Tr number increases. After the transient process, the steady migration velocity

also increases as Tr number increases. To compare with the case of $Ma = 5$ in Fig. 3, the raising rate of the steady migration velocity with Tr number clearly decreases. Figure 6(a) displays the pattern evolution of streamlines in a reference frame moving with the droplet generated by the mirror symmetry and isotherms in a laboratory coordinate system at $Ma = 100$ and $Tr = 5$. To compare with the case of $Ma = 5$ in Fig. 4(a), the computed velocity fields are similar, but the temperature fields are very different. On one hand, at $Ma = 100$, the heat conduction only plays a weak role in the energy redistribution. Although the thermal energy of the interface is still absorbed from the thermal radiation, it is difficult for transferring the thermal energy to both fluids along the normal direction of the interface through the heat conduction. Even at the longer time ($t = 90$), a higher temperature region cannot be formed in both fluids near the top of the droplet. The isotherms

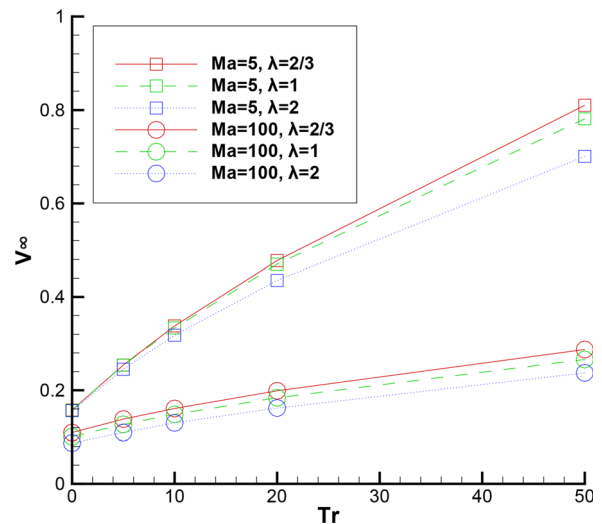


FIG. 8. Steady migration velocity vs Tr number at $Ma = 5, 100,$ and $\rho_2 = \mu_2 = k_2 = 0.8$ and $\lambda(\kappa_2) = 2/3(1.2), 1(0.8), 2(0.4)$.

close to the droplet in the continuous phase fluid bend to the migration direction. Since the droplet cannot obtain enough thermal energy through the heat conduction to rise the internal temperature, the isotherms inside the droplet connect with those behind the droplet and make self-closed lines. A local region with the lower temperature in the droplet is thus formed in the droplet. On the other hand, at $Ma = 100$, the heat convection makes a main role in the energy redistribution. The thermal energy of the interface absorbed from the thermal radiation is transported along the interface by the stronger heat convection. The temperature gradient along the interface is reduced, so that the non-uniform surface tension distribution tends to be uniform. That is the main reason for the decrease in the raising rate of the steady migration velocity with Tr number at $Ma = 100$. To compare

with the case of $Ma = 5$ in Fig. 4(c), Fig. 6(c) shows that at a fixed time the decrease in the interface temperature T_s with θ is still kept, but the absolute value of temperature gradient $|\partial T_s / \partial \theta|$ decreases. As time increases, the shape of curve of T_s with θ is approximately kept, but the growth rate of T_s is lower than that in Fig. 4(c). It reveals that the normal surface tension module changes with t but the tangential surface tension approximately does not change. In Fig. 6(f), as time increases, the total normal surface force $F_{\sigma n, \bar{z}}$ approaches a constant. At each time, the total normal surface force $F_{\sigma n, \bar{z}}$ and the total tangential surface force $F_{\sigma t, \bar{z}}$ are approximately opposite numbers to each other.

Figure 6(b) displays the streamlines in a reference frame moving with the droplet generated by the mirror symmetry and isotherms in a

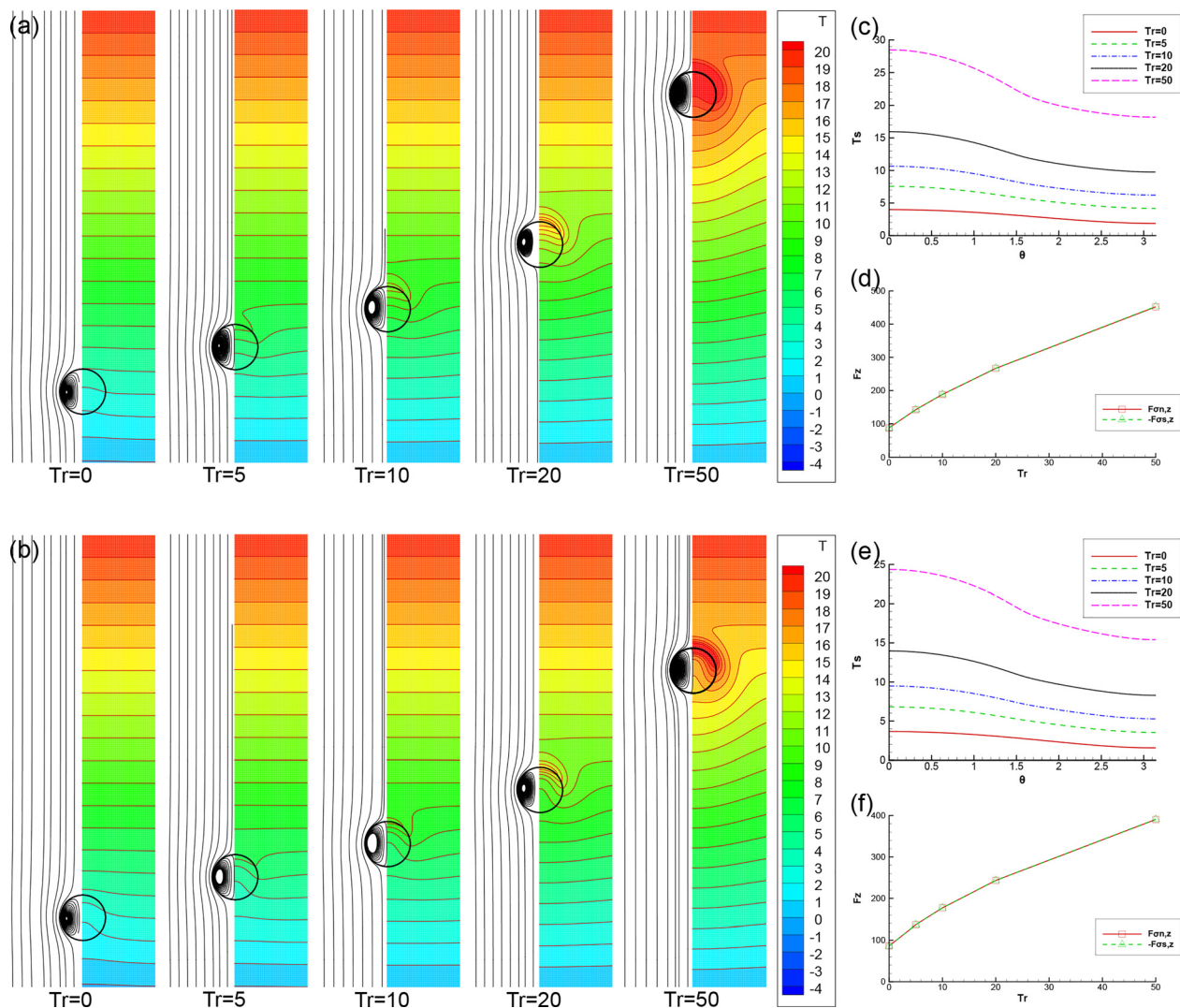


FIG. 9. Streamlines in the reference frame moving with the droplet generated by the mirror symmetry and isotherms in a laboratory coordinate frame at $Tr = 0, 5, 10, 20$, and 50 and the fixed $t = 20$ for $Ma = 5, Pr = 50, Ca = 0.1, \rho_2 = \mu_2 = k_2 = 0.8$ and (a) $\lambda(\kappa_2) = 2/3(1.2)$; (b) $\lambda(\kappa_2) = 2(0.4)$. The correspondent interface temperature T_s vs θ and the total normal (tangential) surface force $F_{\sigma n, \bar{z}}$ ($-F_{\sigma t, \bar{z}}$) on the droplet projected to the \bar{z} direction vs Tr are drawn in (c) and (d) and (e) and (f), respectively.

laboratory coordinate system at the steady migration state ($t = 50$) for $Ma = 100$ and $Tr = 0, 5, 10, 20,$ and 50 . As Tr number increases, an adding temperature gradient along the interface enhances the non-uniform surface tension distribution, so the larger driving force accelerates the droplet to move up. Although the most of thermal energy of the interface absorbed from the thermal radiation is transported along the interface due to the stronger heat convection, a small amount of the thermal energy obtained from thermal radiation is confined in the local region of both fluids near the upper hemisphere due to the weaker heat conduction. At larger Tr number (≥ 50), a higher temperature region is formed in both fluids near the top of the droplet. At this case, the isotherms close to the droplet in the continuous phase fluid bend to the downstream direction

along the interface. In the droplet, the thermal energy, which flows into and out of the droplet through the heat conduction, is transferred by the heat convection. The self-closed isotherms in the droplet are thus formed. To compare with the case of $Ma = 5$ in Fig. 4(e), Fig. 6(e) shows that although both the interface temperature T_s and the absolute value of temperature gradient $|\partial T_s / \partial \theta|$ still increase as Tr increases, their growth rates are lower than those in Fig. 4(e). It reveals that both the normal and the tangential surface tension modules change with Tr . As shown in Fig. 6(f), the total normal surface force $F_{\sigma n, \bar{z}}$ monotonously increases with the increasing of Tr . At each Tr , the total normal surface force $F_{\sigma n, \bar{z}}$ and the total tangential surface force $F_{\sigma \tau, \bar{z}}$ are approximately opposite numbers to each other.

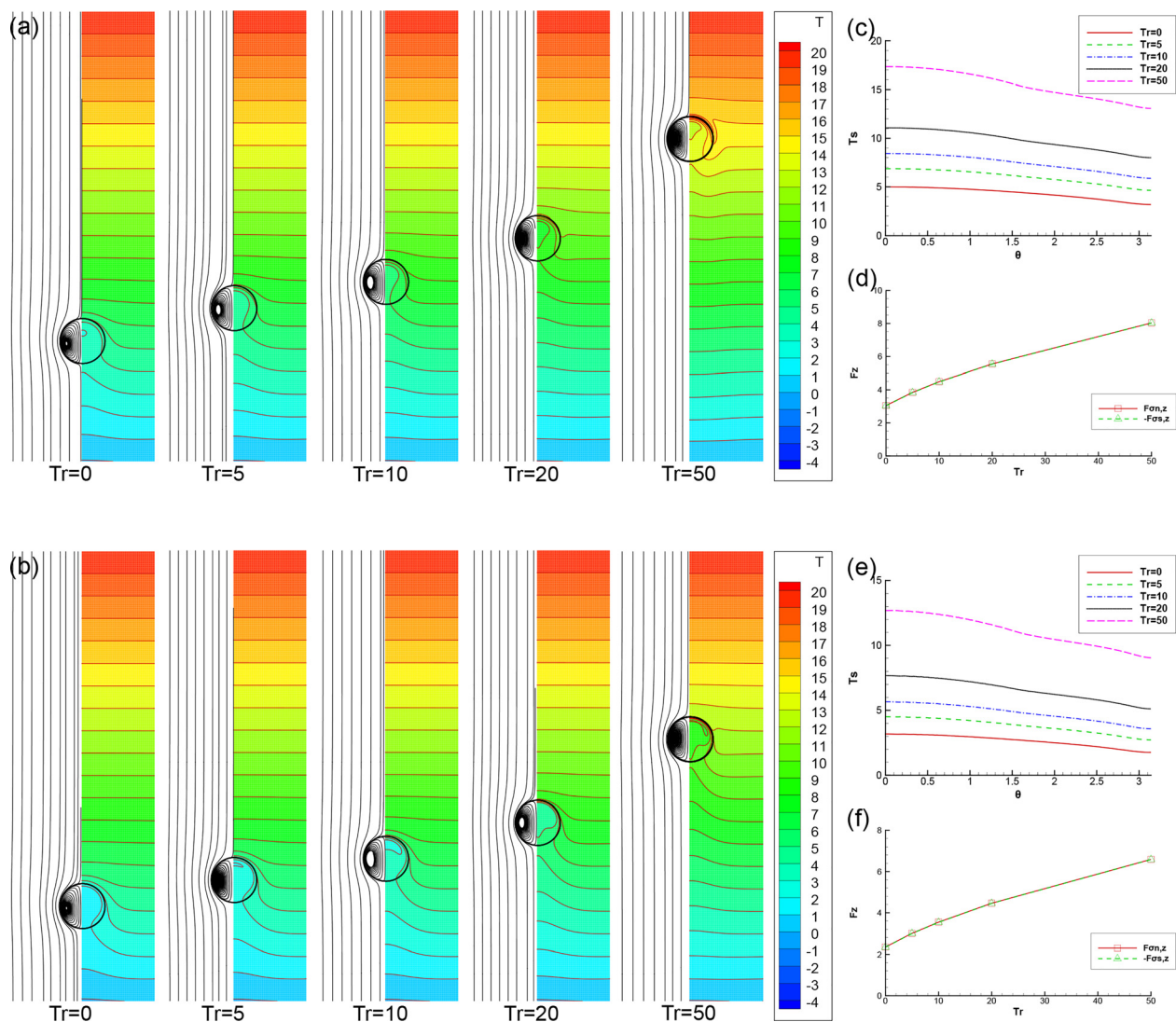


FIG. 10. Streamlines in the reference frame moving with the droplet generated by the mirror symmetry and isotherms in a laboratory coordinate frame at $Tr = 0, 5, 10, 20,$ and 50 and the fixed $t = 50$ for $Ma = 100, Pr = 50, Ca = 0.1,$ and $\rho_2 = \mu_2 = k_2 = 0.8$ and (a) $\lambda(\kappa_2) = 2/3(1.2)$; (b) $\lambda(\kappa_2) = 2(0.4)$. The correspondent interface temperature T_s vs θ and the total normal (tangential) surface force $F_{\sigma n, \bar{z}}$ ($-F_{\sigma \tau, \bar{z}}$) on the droplet projected to the \bar{z} direction vs Tr are drawn in (c) and (d) and (e) and (f), respectively.

Figure 7(a) displays the dependence of the steady migration velocity V_∞ on Ma number for $Tr = 0, 5, 10, 20$, and 50 . In the range of Tr number, V_∞ decreases as Ma number increases. The descent rate of V_∞ with Ma number is larger when Tr number is larger. Figure 7(b) displays the dependence of steady migration velocity V_∞ on Tr number for $Ma = 1, 5, 20, 50$, and 100 . In the range of Ma numbers, V_∞ increases as Tr number increases. The raising rate of V_∞ with Tr number is smaller when Ma number is larger.

2. Effects of the volume heat capacity ratio on thermocapillary droplet migration

In the continuous phase fluid, thermal energy can be transported from the external field and the interface by the heat convection and the heat conductivity. However, in the droplet, thermal energy can be only transported from the interface by the heat conductivity. When the radiative heat energy is absorbed by the interface of the upper hemisphere, the temperature of interface is higher than these of the continuous phase fluid and the droplet near the interface. The intensity of heat energy transferred from the interface to both fluids, which depends on their physical parameters, can affect on the redistribution of the temperatures in both fluids and the pattern evolution of isotherms. In the Sec. IV B 1, due to the non-dimensionalized parameters $k_2 = \kappa_2 = 0.8$, the dimensional volume heat capacity of both fluids are the same ($\rho_1 C_1 = k_1/\kappa_1 = \rho_2 C_2 = k_2/\kappa_2$). For convenience, the volume heat capacity ratio between the droplet and the continuous-phase fluid is defined as

$$\lambda = \frac{\rho_2 C_2}{\rho_1 C_1} = \frac{k_2/\kappa_2}{k_1/\kappa_1} = \frac{k_2/k_1}{\kappa_2/\kappa_1}, \tag{37}$$

which is also the non-dimensionalized volume heat capacity of the droplet ($\lambda = \rho_2 C_2 = k_2/\kappa_2$). In the energy equation (27), for $\lambda = 1$, the adding radiation heat energy to both fluids are the same. In the following, we will investigate thermocapillary droplet migration for different volume heat capacity ratios λ through changing κ_2 and keeping $k_2 = 0.8$.

The dependence of steady migration velocity V_∞ on Tr number for $Ma = 5$ and 100 with $\lambda(\kappa_2) = 2/3(1.2), 1(0.8)$, and $2(0.4)$ is shown in Fig. 8. For $Ma = 5$, when $Tr = 0$, that is, without the thermal radiation, the steady migration velocities V_∞ are almost the same for the different λ . When $Tr > 0$, V_∞ decreases as λ increases. The descent rate of V_∞ with λ is larger when Tr number is larger. Figures 9(a) and 9(b) display the streamlines in a reference frame moving with the droplet generated by the mirror symmetry and isotherms in a laboratory coordinate system at the steady migration state ($t = 20$) for $Ma = 5$; $Tr = 0, 5, 10, 20$, and 50 ; and $\lambda = 2/3, 2$, respectively. Since the computed velocity fields are similar to those for $\lambda = 1$ in Fig. 4(b), we only focus on the evolution of the temperature fields of the two-phase fluids. At $Ma = 5$, the heat convection plays an equal role as the heat conduction in the energy redistribution. To compare with the case of $\lambda = 1$ in Fig. 4(b), the temperature distributions in the continuous-phase fluids are similar. However, the intensity of heat energy transferred from the interface to the droplet decreases as λ increases. It corresponds to the different contribution of the volume heat capacity ratio to both fluids in the energy equation (27). More and more heat is transferred into the droplet when λ is smaller. It leads to decrease in the bulge of isotherm in the droplet. In comparison with

the case of $\lambda = 1$ in Fig. 4(e), Figs. 9(c) and 9(e) show that although both the interface temperature T_s and the absolute value of temperature gradient $|\partial T_s/\partial \theta|$ increase as Tr increases, their growth rates decrease as λ increases. It reveals that both the normal and the tangential surface tension modules change with Tr . As shown in Figs. 9(d) and 9(f), the total normal surface force $F_{\sigma n, \bar{z}}$ monotonously increases with the increasing of Tr . In comparison with the case of $\lambda = 1$ in Fig. 4(f), the growth rate of $F_{\sigma n, \bar{z}}$ with respect Tr decreases as λ increases. At each Tr , the total normal surface force $F_{\sigma n, \bar{z}}$ and the total tangential surface force $F_{\sigma \tau, \bar{z}}$ are approximately opposite numbers to each other.

In Fig. 8, for $Ma = 100$, the steady migration velocity V_∞ decreases as λ increases. The descent rate of V_∞ with λ is almost constant as Tr number increases. Figures 10(a) and 10(b) display the streamlines in a reference frame moving with the droplet generated by the mirror symmetry and isotherms in a laboratory coordinate system at the steady migration state ($t = 50$) for $Ma = 5$; $Tr = 0, 5, 10, 20$, and 50 ; and $\lambda = 2/3, 2$, respectively. Since the computed velocity fields are similar to those for $\lambda = 1$ in Fig. 6(b), we only focus on the evolution of the temperature fields of the two-phase fluids. At $Ma = 100$, the heat convection is stronger than heat conduction. To compare with the case of $\lambda = 1$ in Fig. 6(b), the temperature distributions in the continuous-phase fluids are similar. However, the intensity of thermal energy transferred from the interface to the droplet decreases as λ increases. It corresponds to the different contributions of the volume heat capacity ratio to both fluids in the energy equation (27). At small λ , more heat is transferred into the droplet. Meanwhile, the thermal energy in the droplet is redistributed by the stronger heat convection. This leads to the formation of the self-closed isotherms in the droplet. In comparison with the case of $\lambda = 1$ in Fig. 6(e), Figs. 10(c) and 10(e) show that although both the interface temperature T_s and the absolute value of temperature gradient $|\partial T_s/\partial \theta|$ increase as Tr increases, their growth rates decrease as λ increases. It reveals that both the normal and the tangential surface tension modules change with Tr . As shown in Figs. 10(d) and 10(f), the total normal surface force $F_{\sigma n, \bar{z}}$

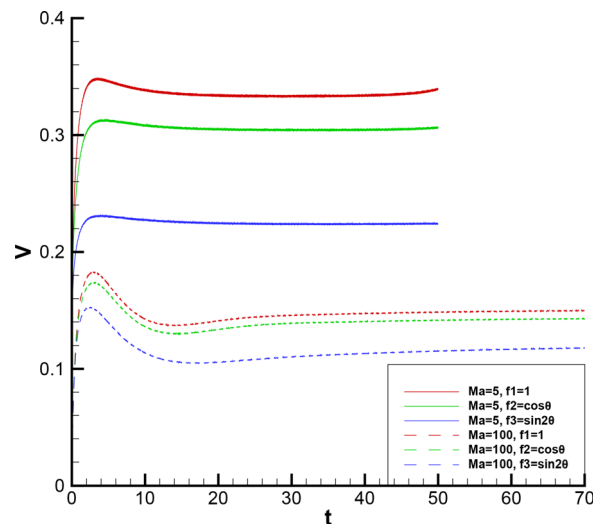


FIG. 11. Time evolutions of droplet migration velocities under the uniform and non-uniform thermal radiations with $f_1 = 1, f_2 = \cos \theta$ and $f_3 = \sin^2 \theta$ at $Ma = 5$ and $100, Tr = 10$, and $\rho_2 = \mu_2 = k_2 = \kappa_2 = 0.8$.

monotonously increases with the increasing of Tr . In comparison with the case of $\lambda = 1$ in Fig. 6(f), the growth rate of $F_{\sigma n, \bar{z}}$ with respect Tr decreases as λ increases. At each Tr , the total normal surface force $F_{\sigma n, \bar{z}}$ and the total tangential surface force $F_{\sigma t, \bar{z}}$ are approximately opposite numbers to each other.

3. Effects of the non-uniform thermal radiation on thermocapillary droplet migration

In Fig. 1(a), when the uniform thermal radiation with $f_1(\theta) = 1$ is replaced by the non-uniform thermal radiations with $f_2(\theta) = \cos \theta$

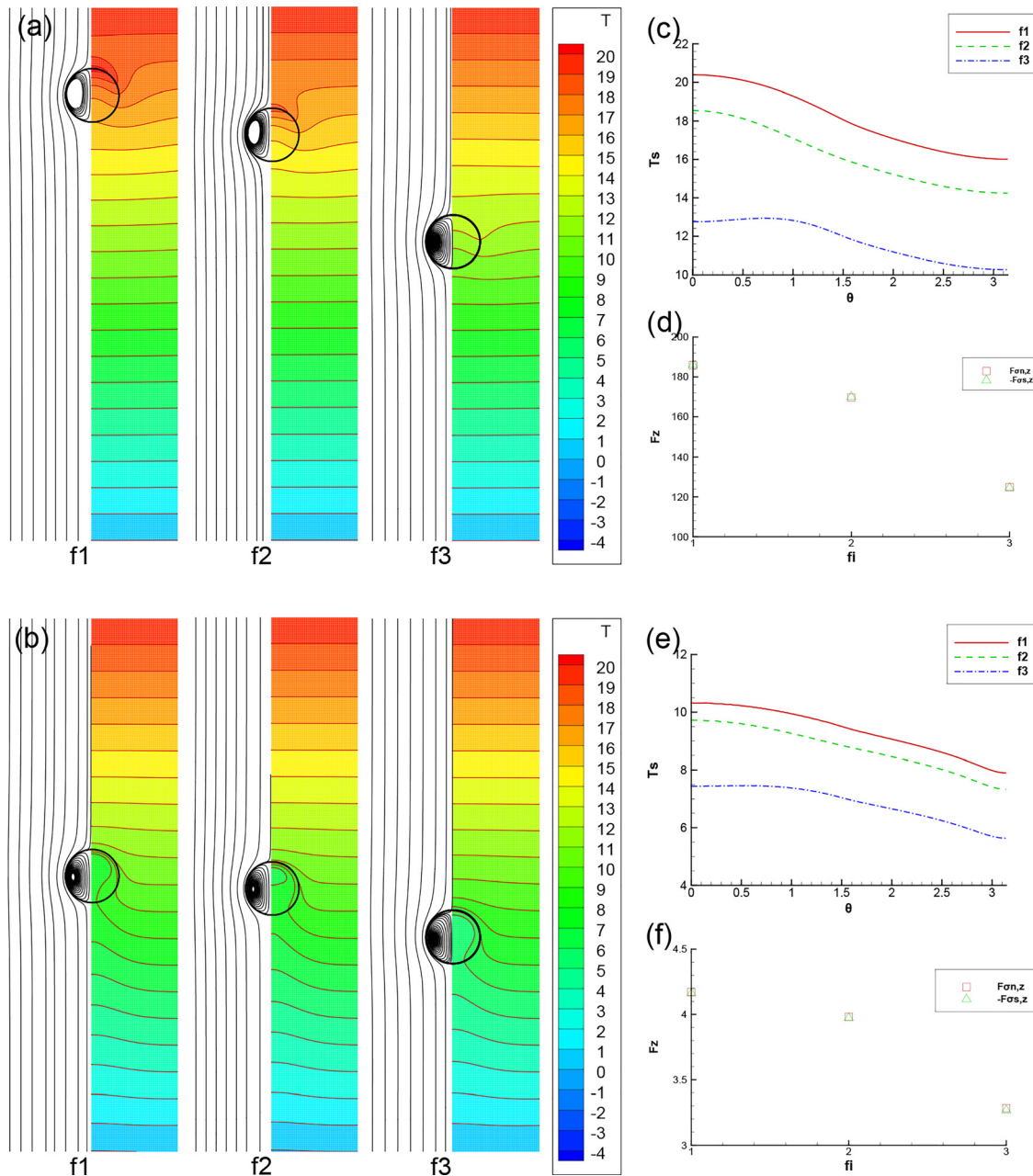


FIG. 12. Streamlines in the reference frame moving with the droplet generated by the mirror symmetry and isotherms in a laboratory coordinate frame under the uniform and non-uniform thermal radiations with $f_1 = 1$, $f_2 = \cos \theta$, and $f_3 = \sin^2 \theta$ for $Pr = 50$, $Ca = 0.1$, $Tr = 10$, and $\rho_2 = \mu_2 = k_2 = \kappa_2 = 0.8$ (a) at $Ma = 5$ and the fixed $t = 50$; (b) at $Ma = 100$ and the fixed $t = 70$. The correspondent interface temperature T_s vs θ and the total normal (tangential) surface force $F_{\sigma n, \bar{z}}$ ($-F_{\sigma t, \bar{z}}$) on the droplet projected to the \bar{z} direction vs f_i are drawn in (c) and (d) and (e) and (f), respectively.

Downloaded from http://pubs.aip.org/aip/pof/article-pdf/doi/10.1063/5.0082867/1663823/1022109_1_online.pdf

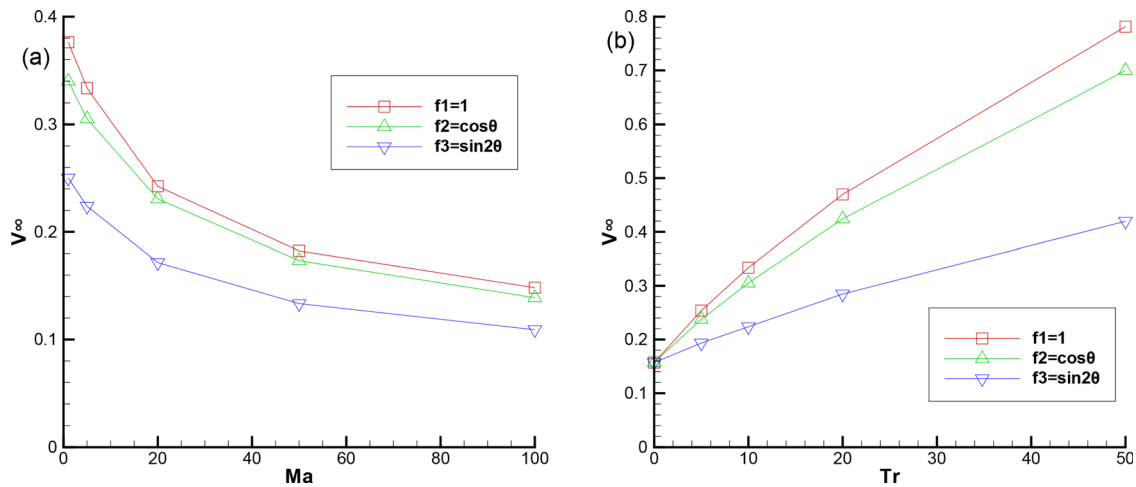


FIG. 13. (a) Steady migration velocity vs Ma number at $Tr = 10$; (b) steady migration velocity vs Tr number at $Ma = 5$ under the uniform and non-uniform thermal radiations with $f_1 = 1$, $f_2 = \cos \theta$, and $f_3 = \sin^2 \theta$.

and $f_3(\theta) = \sin^2 \theta$, respectively, the radiation heat energy functions in Eq. (29) are written as

$$\delta q_2 = \frac{\cos^3 \theta_A - \cos^3 \theta_B}{3r_c \Delta \bar{r} \Delta \bar{z}} \approx \frac{\sin \theta_A \cos^2 \theta_A \Delta \theta_{AB}}{r_c \Delta \bar{r} \Delta \bar{z}} = \cos \theta_A \delta q_1, \quad (38)$$

and

$$\delta q_3 = \frac{\sin^4 \theta_B - \sin^4 \theta_A}{4r_c \Delta \bar{r} \Delta \bar{z}} \approx \frac{\sin^3 \theta_A \cos \theta_A \Delta \theta_{AB}}{r_c \Delta \bar{r} \Delta \bar{z}} = \sin^2 \theta_A \delta q_1. \quad (39)$$

The time evolutions of the droplet migration velocities under the vertical temperature gradient and the uniform/non-uniform thermal radiations at $Ma = 5$ and 100 , $Tr = 10$ are shown in Fig. 11. Under the non-uniform thermal radiations with f_2 and f_3 , two stages (acceleration and steady) for $Ma = 5$ and three stages (acceleration, deceleration, and steady) for $Ma = 100$ appear in the droplet migration processes, which are similar to those under the uniform thermal radiation with f_1 for $Ma = 5$ and 100 , respectively. The global migration velocities of the droplet under the non-uniform thermal radiations with f_2 and f_3 are smaller than that under the uniform thermal radiation with f_1 . For $Ma = 5$, the streamlines in a reference frame moving with the droplet generated by the mirror symmetry and isotherms in a laboratory coordinate system at the steady migration state ($t = 50$) are shown in Fig. 12(a). Since the computed velocity fields for f_1, f_2 , and f_3 are similar, we only focus on the evolution of the temperature fields of the two-phase fluids. From f_1 to f_2 to f_3 , the droplet is placed at the lower temperature zone and the higher temperature belt in both fluids along the normal direction of the interface gradually decreases. Figure 12(c) shows that the interface temperature T_s decreases from f_1 to f_2 to f_3 . However, the distributions of T_s on the droplet for f_1, f_2 , and f_3 are different. T_s monotonously decreases as θ increases for f_1 and f_2 , but T_s undergoes increasing and decreasing processes as θ increases for f_3 . It reveals that both the normal and the tangential surface tension modules change with f_i . As shown in Fig. 12(d), the total normal surface force $F_{\sigma n, \bar{z}}$ decreases from f_1 to f_2 to f_3 . At each f_i , the total normal surface force $F_{\sigma n, \bar{z}}$ and the total tangential surface force $F_{\sigma t, \bar{z}}$ are approximately opposite numbers to each other.

For $Ma = 100$, the streamlines in a reference frame moving with the droplet generated by the mirror symmetry and isotherms in a laboratory coordinate system at the steady migration state ($t = 70$) are shown in Fig. 12(b). Both the computed velocity and temperature fields for f_1, f_2 and f_3 are similar. To compare with the case of $Ma = 5$ in Fig. 12(c), Fig. 12(e) displays that both the variations of the interface temperature T_s and the absolute value of temperature gradient $|\partial T_s / \partial \theta|$ with f_i are kept. However, the change rate in the increasing/decreasing zone of T_s on the droplet is lower than that in Fig. 12(c). It reveals that both the normal and the tangential surface tension modules change with f_i . In Fig. 12(f), the total normal surface force $F_{\sigma n, \bar{z}}$ decreases from f_1 to f_2 to f_3 . At each f_i , the total normal surface force $F_{\sigma n, \bar{z}}$ and the total tangential surface force $F_{\sigma t, \bar{z}}$ are approximately opposite numbers to each other.

Figure 13(a) displays the dependence of steady migration velocity V_∞ on Ma number for f_1, f_2 , and f_3 at $Tr = 10$. The global evolutions of V_∞ with Ma number for f_2 and f_3 , that is, the monotonically decreasing processes, are similar to that for f_1 . The descent rates of V_∞ with Ma number for f_2 and f_3 are smaller than that for f_1 . At a fixed Ma number, V_∞ for f_2 and f_3 are smaller than that for f_1 . Figure 13(b) displays the dependence of steady migration velocity V_∞ on Tr number for f_1, f_2 , and f_3 at $Ma = 5$. The global evolutions of V_∞ with Tr number for f_2 and f_3 , that is, the monotonically increasing processes, are similar to that for f_1 . The growth rates of V_∞ with Tr number for f_2 and f_3 are smaller than that for f_1 . At a fixed Tr number, V_∞ for f_2 and f_3 are smaller than that for f_1 .

V. CONCLUSIONS AND DISCUSSIONS

In this paper, under controlling by uniform and non-uniform thermal radiations, thermocapillary migration of a droplet in a vertical temperature gradient is theoretically analyzed and numerically investigated. The non-dimensionalized Tr number is proposed to quantitatively depict the intensity ratio of the thermal radiation flux to the uniform temperature gradient. From the momentum and energy equations at zero limits of Re and Ma numbers, analytical results for the uniform and

non-uniform radiation thermal fluxes are determined. The steady migration velocity increases as Tr number increases.

By using the front-tracking method, it is observed that thermocapillary droplet migration under the uniform thermal radiation at moderate Ma and moderate Tr numbers undergoes an acceleration process (and then a deceleration process) and finally reaches a steady process. In the steady migration process, the velocity fields are represented by the non-separated external flow around the droplet and the internal vortex flow in the droplet. In the temperature fields, a higher temperature belt in both fluids near the upper hemisphere is formed. The steady migration velocity decreases with the increasing of Ma number and increases with the increasing of Tr number. Moreover, the intensity of thermal energy transferred from the interface to both fluids depends on the volume heat capacity ratio. For larger/smaller volume heat capacity ratio, more heat is transferred into the continuous phase fluid/the droplet. Furthermore, for the non-uniform thermal radiations, the time evolutions, the structures of temperature fields and parameter dependencies of thermocapillary droplet migration at moderate Ma and moderate Tr numbers are similar to those for the uniform thermal radiation.

This study indicates that the action of thermal radiation can be used to control thermocapillary droplet migration in a vertical temperature gradient, which is of great significance for the understanding of basic mechanisms and practical applications in the microgravity and microfluidic fields.

ACKNOWLEDGMENTS

This research was supported by the National Natural Science Foundation of China through Grants Nos. 11172310 and 11472284 and the CAS Strategic Priority Research Program No. XDB22040403. The author thanks the Institute of Mechanics of CAS research computing facility for assisting in the computation.

AUTHOR DECLARATIONS

Conflict of Interest

The authors confirm that this article content has no conflict of interest.

DATA AVAILABILITY

The data that support the findings of this study are available from the corresponding author upon reasonable request.

REFERENCES

- ¹N. O. Young, J. S. Goldstein, and M. J. Block, "The motion of bubbles in a vertical temperature gradient," *J. Fluid Mech.* **6**, 350 (1959).
- ²R. S. Subramanian, "Slow migration of a gas bubble in a thermal gradient," *AIChE J.* **27**, 646 (1981).
- ³Y. K. Bratukhin, "Thermocapillary drift of a droplet of viscous liquid," *Fluid Dyn.* **10**, 833 (1976).
- ⁴R. Balasubramanian and A.-T. Chai, "Thermocapillary migration of droplets: An exact solution for small Marangoni numbers," *J. Colloid Interface Sci.* **119**, 531 (1987).
- ⁵H. Haj-Hariri, A. Nadim, and A. Borhan, "Effects of inertia on the thermocapillary velocity of a drop," *J. Colloid Interface Sci.* **140**, 277 (1990).
- ⁶R. S. Subramanian, R. Balasubramanian, and G. Wozniak, "Fluid mechanics of bubbles and drops," in *Physics of Fluids in Microgravity*, edited by R. Monti (Taylor & Francis, London, 2001).
- ⁷Z. Yin, Z.-B. Wu, and W. R. Hu, "Thermocapillary migration of drops and bubbles," *Advances in Microgravity Science*, edited by W. R. Hu (Transworld Research Network, Trivandrum, 2009).
- ⁸J. F. Zhao, L. Zhang, Z. D. Li, and W. T. Qin, "Topological structure evolution of flow and temperature fields in deformable drop Marangoni migration in microgravity," *Int. J. Heat Mass Transfer* **54**, 4655 (2011).
- ⁹Z. Yin, L. Chang, W. Hu, Q. Li, and H. Wang, "Numerical simulations on thermocapillary migration of nondeformable droplets with large Marangoni numbers," *Phys. Fluids* **24**, 092101 (2012).
- ¹⁰Y. Albendal, A. Turan, and A. Kalendar, "Thermocapillary migration of an isolated droplet and interaction of two droplet in zero gravity," *Acta Astronaut.* **126**, 265 (2016).
- ¹¹P. Capobianchi, M. Lappa, and M. S. Oliveira, "Walls and domain shape effects on the thermal Marangoni migration of three-dimensional droplets," *Phys. Fluids* **29**, 112102 (2017).
- ¹²S. S. Kalichetty, T. Sundarajan, and A. Pattamatta, "Thermocapillary migration and interaction dynamics of droplets in a constricted domain," *Phys. Fluids* **31**, 022106 (2019).
- ¹³K.-X. Hu, C.-Y. Yan, and Q.-S. Chen, "Instability of thermocapillary-buoyancy convection in droplet migration," *Phys. Fluids* **31**, 122101 (2019).
- ¹⁴X. Luo, Z. Y. Luo, and B. F. Bai, "Effect of thermal convection on thermocapillary migration of a surfactant-laden droplet in a microchannel," *Phys. Fluids* **32**, 092009 (2020).
- ¹⁵S. S. Kalichetty, T. Sundarajan, and A. Pattamatta, "Effect of wall proximity on the lateral thermocapillary migration of droplet rising in a quiescent liquid," *Phys. Fluids* **33**, 022107 (2021).
- ¹⁶D. L. R. Oliver and K. J. DeWitt, "Surface tension driven flows for a droplet in a microgravity environment," *Int. J. Heat Mass Transfer* **31**, 1534 (1988).
- ¹⁷A. Y. Rednikov and Y. S. Ryzantsev, "Thermocapillary motion of a droplet under the action of radiation," *J. Appl. Mech. Tech. Phys.* **30**, 337 (1989).
- ¹⁸P. Lopez, Y. S. Ryzantsev, R. G. Rubio, F. Ortega, M. G. Velarde, J. M. Redondo, "Observation of the thermocapillary motion of a droplet in a laser beam," in *Without Bounds: A Scientific Canvas of Nonlinearity and Complex Dynamics*, edited by R. G. Rubio *et al.* (Springer, Berlin, 2013).
- ¹⁹J. M. Redondo, P. Lopez, O. B. Mahjoub, Y. S. Ryzantsev, and M. G. Velarde, "Thermocapillary and radiative heat flux oscillations," in *Topical Problems of Fluid Mechanics* (Prague, 2014).
- ²⁰Y. S. Ryzantsev, M. G. Velarde, R. G. Rubio, E. Guzman, F. Ortega, and P. Lopez, "Thermo- and soluto-capillarity: Passive and active drops," *Adv. Colloid Interface Sci.* **247**, 52 (2017).
- ²¹B. Zhang, D. Liu, Y. Chen, J. Xu, and Y. Sui, "Numerical investigation on spontaneous droplet/bubble migration under thermal radiation," *Int. J. Therm. Sci.* **129**, 115 (2018).
- ²²J.-H. Gao and Z.-B. Wu, "Steady thermocapillary droplet migration under thermal radiation with a uniform flux," *Microgravity Sci. Technol.* **33**, 5 (2021).
- ²³K. T. Kotz, K. A. Noble, and G. W. Faris, "Optical microfluidics," *Appl. Phys. Lett.* **85**, 2658 (2004).
- ²⁴Y. Kanamori and Y. Otani, "Driving droplet by photo-thermal Marangoni convection," in *Proceedings of the International Symposium on Optomechtronics Technologies*, Paris (2012).
- ²⁵A. T. Ohta, A. Jamshidi, J. K. Valley, H.-Y. Hsu, and M. C. Wu, "Optically actuated thermocapillary movement of gas bubble on an absorbing substrate," *Appl. Phys. Lett.* **91**, 074103 (2007).
- ²⁶T. H. Ting, Y. F. Yap, N.-T. Nguyen, T. N. Wong, J. C. Chai, and T. Yabas, "Thermally mediated breakup of drops in microchannels," *Appl. Phys. Lett.* **89**, 234101 (2006).
- ²⁷V. Pratap, N. Moumen, and R. S. Subramanian, "Thermocapillary motion of a liquid drop on a horizontal solid surface," *Langmuir* **24**, 5185 (2008).
- ²⁸H.-B. Nguyen and J.-C. Chen, "A numerical study of thermocapillary migration of a small liquid droplet on a horizontal solid surface," *Phys. Fluids* **22**, 062102 (2010).
- ²⁹J. P. Delville, M. R. Vincent, R. D. Schroll, H. Chraïbi, B. Isenmann, R. Wunenburger, D. Lasseux, W. W. Zhang, and E. Brasselet, "Laser microfluidics: Fluid actuation by light," *J. Opt. A: Pure Appl. Opt.* **11**, 034015 (2009).
- ³⁰M. Robert, S. Vincent, and J. P. Delville, "Microfluidic transport driven by opto-thermal effects," in *Advanced Microfluidics*, edited by R. T. Kelly (InTech, 2012), Chap. 1.
- ³¹S. Rybalko, N. Magome, and K. Yoshikawa, "Forward and backward laser-guided motion of an oil droplet," *Phys. Rev. E* **70**, 046301 (2004).

- ³²C. N. Baroud, J. P. Delville, F. Gallaire, and R. Wunenburger, "Thermocapillary value for droplet production and sorting," *Phys. Rev. E* **75**, 046302 (2007).
- ³³M. R. Vincent and J. P. Delville, "Thermocapillary migration in small-scale temperature gradients: Application to optofluidic discerning," *Phys. Rev. E* **85**, 026310 (2012).
- ³⁴C. Song, J. K. Moon, K. Lee, K. Kim, and H. K. Pak, "Breathing, crawling, budding and splitting of a liquid droplet under laser heating," *Soft Matt.* **10**, 2679 (2014).
- ³⁵B. A. Bezuglyi and N. A. Ivanova, "Creation, transportation and coalescence of liquid drops by means of a light beam," *Fluid Dyn.* **41**, 278 (2006).
- ³⁶N. A. Ivanova and B. A. Bezuglyi, "Droplet formation in a thin layer of a two-component solution under the thermal action of laser radiation," *Colloid J.* **69**, 735 (2007).
- ³⁷R. Shukla and K. A. Sallam, "Effect of liquid transparency on laser-induced motion of drops," *J. Fluid Eng.* **131**, 081301 (2009).
- ³⁸K. A. Tatosova, A. Y. Malyuk, and N. A. Ivanova, "Droplet formation caused by laser-induced surface-tension-driven flows in binary liquid mixtures," *Colloid Surf. A* **521**, 22 (2017).
- ³⁹Z.-B. Wu and W. R. Hu, "Effects of Marangoni numbers on thermocapillary droplet migration: Constant for quasi-steady state?," *J. Math. Phys.* **54**, 023102 (2013).
- ⁴⁰Z.-B. Wu, "Steady thermocapillary migration of a droplet in a uniform temperature gradient combined with a radiation energy source at large Marangoni numbers," *Phys. Rev. E* **98**, 013110 (2018).
- ⁴¹Z.-B. Wu, "Thermocapillary migration of a droplet with a thermal source at large Reynolds and Marangoni numbers," *Int. J. Heat Mass Transfer* **75**, 704 (2014).
- ⁴²J. Happel and H. Brenner, *Low Reynolds Number Hydrodynamics* (Prentice-Hall, Englewood Cliffs, NJ, 1965).
- ⁴³Z.-X. Wang and D.-R. Guo, *Introduction to Special Functions* (Science Press, Beijing, 1979).
- ⁴⁴G. Tryggvason, B. Bunner, A. Esmaeeli, D. Juric, N. Al-Rawahi, W. Tauber, J. Han, S. Nas, and Y. Jan, "A front-tracking method for the computations of multiphase flow," *J. Comput. Phys.* **169**, 708 (2001).
- ⁴⁵C. S. Peskin, "Numerical analysis of blood flow in the heart," *J. Comput. Phys.* **25**, 220 (1977).
- ⁴⁶Z.-B. Wu and W. R. Hu, "Thermocapillary migration of a planar droplet at moderate and large Marangoni numbers," *Acta Mech.* **223**, 609 (2012).